

Department of Precision and Microsystems Engineering

ADAPT: A 3 Degrees of Freedom Reconfigurable Force Balanced Parallel Manipulator for Aerial Applications

Kartik Suryavanshi

Report no : 2022.054
Coaches : Dr.ir. V. van der Wijk, Dr. Salua Hamaza
Professor : Prof.dr.ir. J.L. Herder
Specialisation : Mechatronic System Design
Type of report : Master Thesis
Date : 29 September 2022

ADAPT: A 3 Degrees of Freedom Reconfigurable Force Balanced Parallel Manipulator for Aerial Applications

by

K.Suryavanshi

to obtain the degree of Master of Science
at the Delft University of Technology,
to be defended publicly on Monday Sept 29th, 2022 at 02:30 PM.

Student number: 5023335
Project duration: September 1, 2021 – September 29, 2022
Thesis committee: Dr. ir. V.v.d Wijk, TU Delft, supervisor
Dr. S.Hamaza, TU Delft, co-supervisor
Prof. dr. ir. J. Herder, TU Delft, chair

An electronic version of this thesis is available at <http://repository.tudelft.nl/>.

Preface

The thesis is a result of a year-long fortuitous research journey at the TU Delft. I have always been inclined to do research in a field that involved purely mechanical engineering concepts and was very lucky to find this topic and make something good of it. The research was mentally very rewarding and I was never at a loss for any thoughts as there were always some challenging problems to solve. I enjoyed the research phase thoroughly and especially the visual nature of the problems in this project about which I could think even during my off-screen time at the gym or after naps. I would have not known this topic unless I had taken the course Precision Mechanism Design. For this, first of all, I would like to thank Prof. Just Herder. This course was very engaging and that's how I got introduced to the work of Volkert.

I am grateful to Ad Huisjes who connected me with Volkert. I cannot describe how fortunate I feel to have worked with Volkert. Coming from India, where there is always an unsaid hierarchy, it was very refreshing to work with Volkert who behaved more like an experienced colleague and a friend. This enabled many jovial conversations and the meetings were always fun. Apart from all the jovial conversations, project discussions with him were very engaging and he always gave me tremendous insights. These insights helped me stay in the right direction and on schedule and helped shape the project. There were times when I doubted myself if I could do some things on my own, Volkert always made me believe that there were no limits to my capabilities and this helped me solve the problems on my own.

I am thankful to Dr.Salua Hamaza who helped guide the project in the right direction. Salua's input on the use of manipulators on drones expanded the scope of this project and at the same time provided the right constraints for the design of the manipulator. I am grateful to her for helping me find a spot at the aerospace faculty and help with experiments at the Cyber Zoo.

I am grateful to all the supervisors at the IWS workshop for being patient with me despite me not knowing any manufacturing machines in the beginning. Their design inputs and their readiness to help me all the time helped me endure the three months I spent at the workshop.

I would also like to thank my friends without whom I would have lost my sanity on this year-long journey. I would not name them all but everyone of them had a big part in helping me finish my thesis.

Lastly, I would like to thank my family who has supported me in all my decisions and been a pillar of strength for me all the time. I am forever grateful to them for all the sacrifices they have made to give me a chance for a better future.

*K.Suryavanshi
Delft, September 2022*

Contents

List of Figures	iii
Glossary	iv
1 Introduction	1
1.1 Motivation	1
1.2 Prior art	2
1.3 Problem definition	2
1.4 Research goal and objectives	3
1.5 Thesis outline	3
2 Methods for designing inherently dynamically balanced mechanisms and their comparison	4
3 ADAPT: A 3 Degree of Freedom Reconfigurable Force Balanced Parallel Manipulator for Aerial Applications	13
4 Discussion	26
4.1 Discussion	26
4.2 Recommendations for Future Work	27
5 Conclusion	29
Bibliography	31
A Design Considerations	32
B Kinematics (Elaborated)	35
C Workspace	40
C.1 Analytical Workspace Estimation without the drone body	40
C.2 Computer Assisted Manual Optimization	41
D Simulations on a pantograph and further simplified model of ADAPT	43
D.1 Pantograph	43
D.2 Further simplified model	44
E LabVIEW Block Diagram and User Interface	45

List of Figures

1.1	The Butterfly effect is a highly used metaphorical example to explain the chaos theory. [1]	1
1.2	Family of balanced four bar mechanisms developed at the Laval University were primarily used to develop reactionless mechanisms [13]	2
1.3	Balanced PAMINSA Manipulator. One of the few spatial manipulators where the dynamics are considered at the system level. [24]	2
4.1	The force balanced planar 3-RRR operation mode	28
4.2	The force-balanced spherical parallel 3-RRR operation mode	28
4.3	Schematic model of active balancing units. Motors have not been included but can be fixed to counterweights. a)One balancing element for each DoF b)One balancing element for all DoFs [27]	28
A.1	General 2-DoF pantograph structure with the centre of mass of the structure at point S. The pantograph is mass symmetric about the instantaneous line joining points A and S. Since the legs are mass symmetric therefore the q's have a value of zero.	32
A.2	Nomenclature of the various components used in the table.	34
B.1	Schematic diagram of one of the legs with the kinematic parameters.	35
B.2	Schematic diagram of one of the legs with the kinematic parameters. When all the joints are kept fixed and only ϕ_{3i} is allowed to move then the leg end point forms a circle with a fixed radius. This radius (C) is independent of the joint variable ϕ_{3i}	37
C.1	Planar reach limits of one of the legs. The workspace solid volume can be found by revolving the surface S around the central axis.	40
C.2	Left:Planar reach limits of one of the legs. The workspace solid volume can be found by revolving the surface S around the central axis. Right:The workspace shape and volume with the starting values.	41
C.3	Change in the workspace volume with changing parameters. (a) Increasing r, (b) Increasing R, (c) Increasing L_1 , (d) Increasing L_2	41
C.4	Optimized workspace with favorable values	42
D.1	MSC ADAMS model of a forced balanced pantograph. The CoMs of the longer links have been artificially put outside the links so that they fulfill the force balance conditions. The CoM is represented by the frames in MSC ADAMS	43
D.2	Forces in the X direction for a pantograph. The shorter link is turned anti-clockwise in the simulation that extends the arms of the pantograph.	43
D.3	The further simplified model of the manipulator with CoMs put artificially at points where they would exist if there were masses and motors like in the real system.	44
E.1	The LABVIEW block diagram for single channel data acquisition	45
E.2	The LABVIEW User Interface	46

Glossary

List of acronyms

2D	Two Dimensions
3D	Three Dimensions
AEROARMS	Aerial Robotic system integrating multiple Arms
DoF	Degree of Freedom
TU	Technical University
US	United States
UAV	Unmanned Aerial Vehicle

Introduction

1.1. Motivation



Figure 1.1: The Butterfly effect is a highly used metaphorical example to explain the chaos theory. [1]

Until the latter half of the 20th century, it was believed that balance is a law of nature, any small deviation will be corrected by negative feedback that will bring the system back to its original point of balance [2]. We now know that this is incorrect and this theory has been superseded by the chaos theory. Chaos theory, in simple terms, states that a system always leans towards disorder. Comparably, we have also come to realize that the entropy of an isolated system always increases from the second law of thermodynamics [3]. There needs to be a human intervention to change the entropy of the system locally. We as researchers always strive towards bringing order from chaos, decreasing the entropy in effect. Examples include simple concepts like installing traffic lights to smoothen the traffic or complex phenomenon like building models to decipher the stock market or predicting the weather.

Along similar lines, the research presented in this thesis is an endeavor toward conserving the orderliness in a mechanical system. We need mechanical systems that are balanced since unbalanced systems create reaction forces following Newton's third law. These reaction forces lead to noise, wear and fatigue problems [4] and can compromise the accuracy of the machines [5]. In the hi-tech industry, these forces lead to unwanted vibrations that increase the cycle times for processes. In aerial and space vehicles with manipulators, the reaction forces due to the motion of the arms can change the trajectory due to dynamic coupling [6]–[8]. To diminish the effect of these reaction forces, researchers have developed many passive and active dampening methods using externally attached devices. Passive devices like tuned mass dampers and tuned liquid dampers are predominantly used in the dampening of vibrations in large structures[9]. Active control methods are also employed in small structures where the dynamic model is available[10]. As one would notice, these methods act on the reaction forces after they have been created. It is best to have mechanisms where there is no vibration at the source at all. This is possible when the balance of reaction forces is considered during the synthesis of the mechanism. This research focuses on the development of one such mechanism.

1.2. Prior art

There have been many research efforts toward the development of reactionless mechanisms. The necessary and sufficient condition for a mechanism to be reactionless is that the linear momentum should be zero such that the CoM remains stationary (however, this is a stricter definition, a mechanism can also have constant velocity such that its linear momentum remains constant) and angular momentum should remain constant. All the reactionless mechanisms are developed based on these fundamental conditions. One way to do this is to balance the mechanism using additional balancing elements in the design. Wijk et al explore and evaluate various methods of complete dynamic balancing using additional mass and inertia [11]. However, these additional elements whose sole purpose is to balance lead to an increase in mass, and inertia and makes the system more complex. Mechanisms where all the elements contribute to the motion as well as the balancing are better suited in situations where weight is a constraint. These mechanisms are called inherently balanced mechanisms [12] and are elaborated in Chapter 2.

1.3. Problem definition

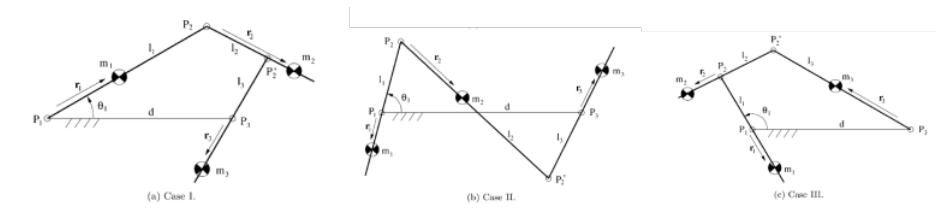


Figure 1.2: Family of balanced four bar mechanisms developed at the Laval University were primarily used to develop reactionless mechanisms [13]

Most of the research efforts have involved the use of balanced mechanisms as elemental entities that are combined to make higher DoFs mechanisms [13]–[18]. This method of balancing leads to mechanisms that are much heavier than their unbalanced counterparts and sometimes very complex to realize in practice. Research works that have considered counterbalancing at the complete system level have been either restricted to planar mechanisms [19]–[23] or have led to the development of just motion decoupled mechanisms and are not reactionless [24]–[26].

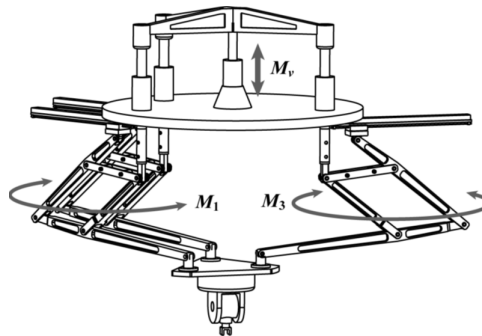


Figure 1.3: Balanced PAMINSA Manipulator. One of the few spatial manipulators where the dynamics are considered at the system level. [24]

PAMINSA manipulator considers manipulator-level spatial force balancing through mass redistribution through its links. However, the design was made with decoupling in mind so it is highly asymmetric. There are only two actuators in three legs for planar translations. The third actuator is put above the leg assembly for vertical translation. The use of horizontal prismatic joints also makes the setup heavy. There are no force-balanced spatial manipulators that consider balancing at the system level to the best of the knowledge of the author.

This also relates to the problem of coupled dynamics in aerial vehicles with manipulators. When manipulators attached to an aerial vehicle move, it leads to reaction forces on the aerial vehicles. To solve this, various complex control methodologies are used. These methods are briefly introduced in Chapter

3. A research gap exists in the design of a manipulator that is decoupled from the aerial vehicle. This leads to the definition of the research goal.

1.4. Research goal and objectives

Although a dynamically balanced manipulator would be ideally the best result that would be a solution to all the aforementioned problems, moment balancing is too hard to realize in practice without significant weight increase. Therefore, the focus is on a smaller problem of force-balancing. Since the research focuses on building a spatial forced balanced manipulator for its use in an aerial vehicle. The research goal is defined as follows

To build a force-balanced spatial translation mechanism for an aerial vehicle

To reach this goal, several objectives are defined:

1. **To develop a concept for the forced balanced manipulator** To develop the model, various concepts of inherently forced balanced mechanisms are explored and compared. The motion capabilities of the existing mechanism, in particular, DYMO is explored, to create a force-balanced mechanism from the same.
2. **Formulation of a kinematics model** Since the design is unique and new, a new kinematic model has to be developed. The position of the active joint after the passive joint is especially problematic in the kinematic sense. It is problematic since the usual analytical ways to find the inverse kinematic model cannot be applied and hence geometrical reduction is done.
3. **Dynamic Simulation, Experimentation, and Validation.** A simplified model of the manipulator is developed to be simulated within the MSC ADAMS environment. The simulation should show that the manipulator is theoretically reactionless. To validate the simulation results, an actual model of the model is built and tested to confirm the results of the simulation.

1.5. Thesis outline

In Chapter 2, the methods of designing inherently balanced mechanisms are explored and compared on various parameters. Chapter 3 discusses the force-balanced manipulator. The design is first presented and its similarity to the DYMO robot is outlined. Next, the kinematic model is formulated which then leads to the definition of singularity and workspace. Simulation and Experiments are done at the end of the Chapter for validation. In Chapter 4 the results are discussed. In the end, the report ends with Conclusion and Recommendations in Chapter 4.

Appendix is also provided after the main report. In Appendix A, the design considerations are presented that would help the reader replicate the design. Since not every step in the development of a kinematics model could be explained in the paper format in Chapter 3, Appendix B elaborates on the kinematic model with all the steps included. In Appendix C, the computer-assisted manual optimization is explained and the preliminary results are presented. Appendix D discusses the simulation on a pantograph to give an idea of the order of numerical error.

2

Methods for designing inherently dynamically balanced mechanisms and their comparison

Methods for designing inherently dynamically balanced mechanisms and their comparison

Kartik Suryavanshi
High-tech Engineering
Tu Delft

Delft, Netherlands
k.suryavanshi@student.tudelft.nl

Abstract—Fast-moving machines generate reaction forces and moments at their base that are undesirable. Additional elements are added to neutralize this effect leading to excessive weight increase which in some cases is not desirable. In this report various inherently force and moment balance techniques are explored and elaborated. These mechanisms do not need additional elements to balance the reaction forces and moment. Every element in these mechanisms serves the dual purpose of balancing and fulfilling the role as a kinematic link. In the end, the methods discussed are compared and a conclusion is presented.

Index Terms—dynamic balancing, principal vectors, inertia tensor

I. INTRODUCTION

It is a well-known fact that moving mechanisms exert reaction forces in the supporting structure leading to noise, wear, and fatigue problems [2]. This has led many researchers to develop reaction-less mechanisms which are dynamically balanced. A mechanism is dynamically balanced if during its motion it exerts no reaction force (excluding the gravitational force) and reaction moments at all times. This is important in space robotics since it helps to maintain the momentum of the moving base in space vehicles. It is also crucial in telescopes as the telescope needs to be moved at a high frequency to correct for the atmospheric disturbances. In the precision industry, dynamic balancing reduces the vibrations thereby decreases the cycle times and also improves the accuracy. [1].

The necessary and sufficient condition for a mechanism to be dynamically balanced is that the linear momentum should be zero such that the center of mass remains stationary and angular momentum should remain constant.

The first class of dynamically balanced mechanisms is the mechanisms that are balanced after the kinematic synthesis. This usually involves the addition of extra elements that increase the mass, the moment of inertia, and makes the system more complex. The research on these classes of mechanisms is very mature and an exhaustive review can be found in the following works [3], [4].

This literature survey predominantly deals with mechanisms that have elements whose function is not solely to move within its kinematic limits but to also help with dynamic balancing. The second class of mechanisms is called inherently dynamically balanced mechanisms [5]. This design approach

of mechanisms allows for systems that have lesser components than the first class of mechanisms and therefore lighter as each element has to fulfill both the kinematic and the dynamic constraints such that the mechanism remains dynamically balanced. This approach also allows for balancing before the kinematic synthesis which fixes the design, unlike the former approach in which the design may have to be changed to make the system dynamically balanced. Looking at the benefits, this literature survey tries to find an answer to the following question 'Which methods exist for inherent dynamic balancing and how do they compare?'.
The report is organized as follows, in Section 2, the fundamental equations for balancing are presented and then the methods are detailed. Next in Section 3, the methods are compared and then the report ends with the conclusion at the end.

II. METHODS

For a system with constant mass, the resultant forces equal the time rate of change of linear momentum and the resultant external moments equals the rate of change of angular momentum about the same point [8],

$$\sum F = m\dot{v} \quad (1)$$

$$\sum M = \dot{h} \quad (2)$$

Where $\sum F$ is the external force vector, m is the total mass, v is the velocity vector of the center of mass, $\sum M$ is the moment about the reference point and h is the total angular momentum vector about the same reference point. If the right-hand side equation (1) is zero and the center of mass is fixed and the right-hand side of equation (2) is zero then the system can be said to be reactionless or dynamically balanced. i.e.

$$\frac{\partial r}{\partial t} = 0 \quad (3)$$

$$\frac{\partial h_o}{\partial t} = 0 \quad (4)$$

where r is the position vector of the center of mass (note that here the CoM is assumed to be fixed, therefore position vector not changing, although this does not need to be the case in general, even CoM moving with constant velocity can be reactionless but these mechanisms are hard to realize in

practice) and h_o is the angular momentum of the mechanism with respect to a generic point o. All the studies on dynamic balancing are based on these fundamental equations and their alterations [9]. In this section, the methods employed to dynamically balance a mechanism that is essentially based on these equations are elaborated.

A. Principal Vectors

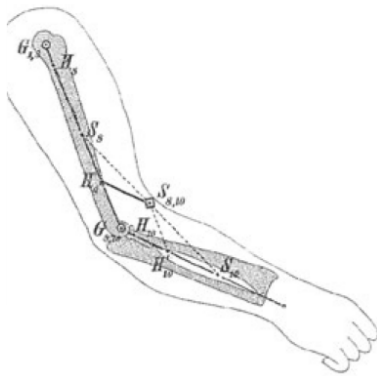


Fig. 1. Fischer's method applied to the right arm [10]

At the turn of the 20th-century German medical doctor, Otto Fischer came up with exemplary work to understand the motion of the human musculoskeletal system and to describe the motion of the center of mass and inertia of body segments. Fischer was interested to derive the individual muscle force for humans in motion but found that the inverse dynamics model of humans at each instant is cumbersome to do by hand. Fischer decided to investigate the motion of body common CoM independently from the relative motions of the body segments with respect to the body CoM. This way the relative motion could be determined from the kinematic model and the dynamic model could be reduced. This reduction step was called the method of principal vectors. Fischer employs this method to derive the equations of motion for various mechanisms in his works [10]. An example of Fischer's vector construction for a hand is shown in Fig.1. The method of principal vectors develops forced balanced mechanisms. To make the mechanism moment balanced as well, the inertia tensor has to be chosen such that it remains constant. An example involving moment balancing is presented later in the section.

The principal vector method consists of principal vector linkages (Fig. 2). Principal vector linkages are forced balanced linkages consisting of principal elements, which are connected by revolute joints called the principal joints. These allow relative motion between the common CoM and the principal elements. Vectors having constant magnitude describe the position of principal points with respect to the common CoM. The force balance conditions, which essentially consist of derivatives of linear momentum equations that are equated to zero, describe the position of principal points within the

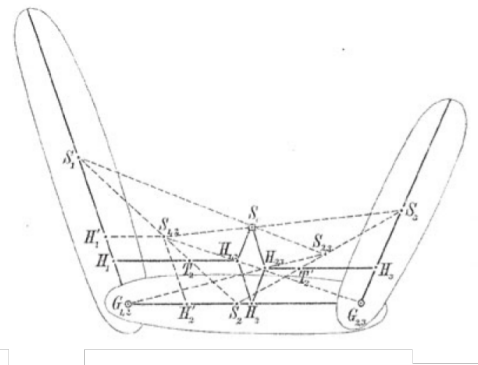


Fig. 2. Principal vector linkage with three elements. Fisher used these kinds of constructions for determination of internal forces without modeling the whole body dynamics [10]

principal elements. Principal vectors describe the position of the principal points with respect to the common CoM. Their magnitudes, which are called principal dimensions, are derived from the force balance conditions as well. Since their lengths are constant, principal vectors are transformed into rigid links, the principal vector links, whose masses are taken into account when the position of the common CoM and the reduced-mass models are defined. It can be stated that in principal vector linkages the CoMs of all the links are related to the common CoM. Force balance is achieved by keeping this point invariant.

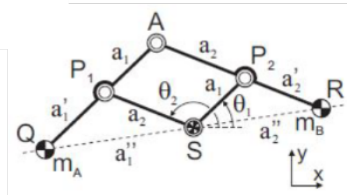


Fig. 3. Pantograph, an elementary forced balanced mechanism, used in construction of inherently dynamically balanced mechanisms [5]

This property is found in pantograph linkages (Fig.3), which is a 2 DoF forced balanced linkage where S is the common CoM and the principal vectors correspond to links SP1 and SP2 having principal dimensions, respectively, a_2 and a_1 . Principal elements AP1 and AP2, having principal points P1 and P2 and CoMs in Q and R, are connected through principal joint A. The reader is referred to the work of Van der Wijk for more elaboration. [5].

Several researchers have used principal vector linkages in the development of various force balanced and gravity compensation devices.

Agrawal introduced the concept of the auxiliary parallelogram which is originally based on Otto Fischer's work and proposed several mechanisms [11]–[16] that are forced balanced and reactionless. He also proposed a graph made of parallelograms

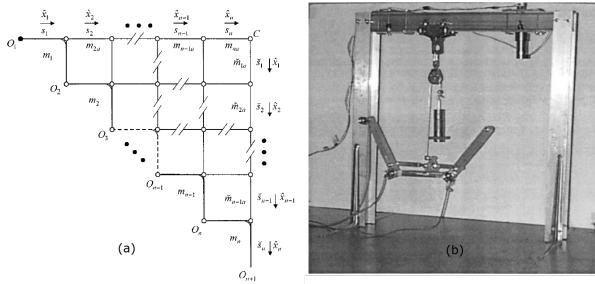


Fig. 4. (a) Graph made of parallelograms to find the CoM of a generic n-link serial chain mechanism. (b) Physical embodiment of a three link principal vector chain with masses of all elements considered [11]

to determine the CoM of a generic serial chain (Fig.4(a)). Quite notable was the development of gravity balanced manipulator which employed Fischer's principal linkage connected to a pin [11]. The common CoM was located at the pin and the pin was made stationary for all the motions. This was the first work that considered the masses of all elements of the principal vector linkage. (Fig.4(b)) In their work on the development of reactionless space robot [13], they show that for a force balanced mechanism, there are two ways to make it moment balanced. First by setting the angular momentum equal to zero and when that is not possible using passive joints such that one or more moment components along an axis are zero. Based on similar concepts they presented a class of reactionless spatial robots [15] where they also fixed the trajectory with additional constraints such that it was moment balanced (Fig.5). However, these mechanisms relied heavily on symmetry. Also, the passive joints, even though do not allow any moments to transfer to the base, would cause undesirable motion of the mechanism.

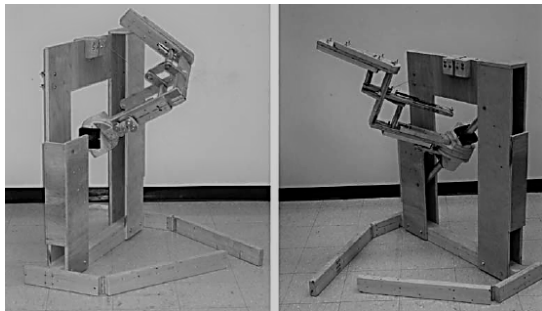


Fig. 5. One of the very few spatial mechanisms, in this case the the mechanism was statically balanced using springs [15]

Alongside, Wijk made significant developments to Fischer's theory of principal vectors. In his works [5] he showed that the force-balanced solutions could be found generically and systematically using the linear momentum equations. He proposed the method of linearly independent linear momentum to derive the force balance conditions for closed-chain mechanisms. He also investigated principal vectors and developed principal vector linkages that were forced balanced. For more than 2

DoF mechanisms he proposed the equivalent linear momentum system to derive the principal dimensions. Wijk also showed how the general angular momentum can be made zero to have shaking moment balance by reducing the DoF. Another way was to design the mechanism in a symmetric manner such that every moving element has a moment countering the moving element. Utilizing this concept of symmetry Wijk developed a force balanced 1 DoF gripper [5](Fig.6). The gripper consisted

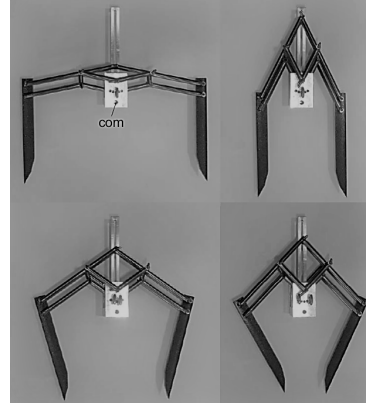


Fig. 6. 1-DoF inherently dynamically balanced grasper mechanism [15]

of a slider that constrained the relative motion between elements much like trajectory control that other research works have proposed. Wijk also developed a Dual V type mechanism by combining two pantographs [30]. The mechanism consisted of 4 limbs symmetrically placed such that the shaking moment generated by each link was in the opposite direction and thus the shaking moment was canceled. One limitation was that the mechanism was completely balanced only when it moved in orthogonal directions. The method of principal vectors although very promising suffers from limitations as it consists of overlapping links. Since the balance mechanism is made of pantographs which are change point mechanisms, when the revolute joints become colinear the mechanism motion cannot be uniquely determined. Although the method is suitable for low DoF force balancing, it quickly becomes complex for higher DoF [17]. Also, moment balancing is quite challenging when non-linear relations among relative DoFs have to be considered. [5]

B. Balanced Four Bar Mechanisms

1) *Momentum Method:* There have been many pioneering works at the Laboratoire de robotique at the Laval University and one of the directions where the lab has excelled is in the development of reactionless (completely dynamically balanced) mechanisms consisting of balanced four-bar mechanisms. In their research works, it is shown that balanced four-bar linkages can be used as elementary entities in the synthesis of planar and spatial reactionless mechanisms. [1], [18]–[20]. In one of the early works they presented two architectures of balanced four-bar mechanisms that were obtained as solutions to the static and dynamic balance equations [18]. These

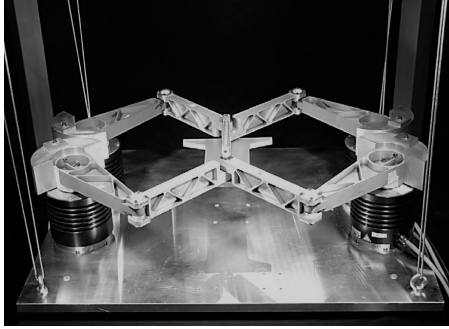


Fig. 7. Dynamically balanced 4RRR DUAL-V mechanism, it can be seen that that the mechanism consists of two balanced pantographs. The mechanism did not require separate counter rotations because of symmetry [30]

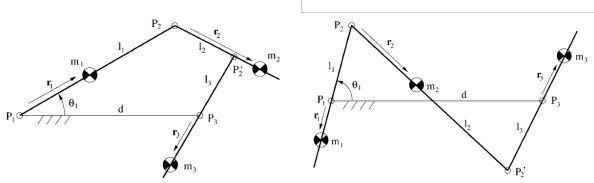


Fig. 8. Dynamically balanced 4 bar mechanisms developed at Laval University, one on the right is called the inverted 4 bar mechanism

designs are shown in Fig.8 These elements were later used in the development of the reactionless planar 3 DoF mechanism. On the same lines, a 3 DoF planar parallel platform was built but with a five-bar mechanism balanced in the same manner as done for the four-bar mechanism [19]. However, the stage in the mechanism was assumed to be very thin and so the dynamic balancing could not be demonstrated in the actual setup. Another exceptional work develops a reactionless 3 DoF and 6 DoF platform using the four-bar mechanisms as elementary blocks without using separate counter-rotating elements. This is one of the first works which shows an inherently balanced spatial mechanism. They show that spatial problem is equivalent to ensuring that the inertia tensor of the reactionless four-bar mechanism remains constant. To develop a 3D mechanism they first develop a chain with a constant inertia tensor and attach another similar chain perpendicularly at its moving link, which is then used to make a 6 DoF mechanism. However, it is mentioned in the paper that the platform is assumed to have zero thickness which is unrealistic. If the platform has a non-zero thickness then the platform has to be replaced by 4 points that are non-coplanar and should then consist of four legs.

2) *Algebraic Method*: The researchers from the same group also presented a new method based on complex numbers to completely characterize force and moment balanced four-bar linkages [20]. It was proven that the set of balanced four-bar mechanisms presented was complete and no additional linkages could be found without adding additional links or counter-rotations. However, this method is not intuitive to a reader with a non-mathematical background and gives little insight into the actual dynamics of the model. The table of

Case	Mode A	Mode B	Mode C
Parallelogram			
$l_1 = l_2 \neq l_3 = d$	$dx_1 x_2 + l_1 x_1 - l_1 x_2 - d = 0$	$x_1 - x_2 = 0$	
Deltoid-1			
$l_1 = l_2 \neq l_3 = d$	$-dx_1 x_2 - dx_1 + l_1 x_2 + l_1 x_1^2 = 0$	$x_2 + 1 = 0$	
Deltoid-2			
$l_1 = d \neq l_2 = l_3$	$dx_1 x_2 + l_1 x_1 - dx_2 - l_1 x_2^2 = 0$	$x_1 - 1 = 0$	
Rhomboid			
$l_1 = l_2 = l_3 = d$	$x_1 - x_2 = 0$	$x_1 - 1 = 0$	$x_2 + 1 = 0$

Fig. 9. All the set of kinematic modes derived for 4 bar mechanism

the derived set of mechanisms is shown in Fig.9

C. Reactionless Path Planning and Constraining Multi DoF

Many research works are concerned with optimum motion planning to achieve dynamic balancing conditions. To be precise, once force balance is achieved, control methods are utilized to make the system moment- balanced. One of the early works involves the design of a nine link redundant manipulator with three actuators sharing a common axis that rotates in opposite direction [24](Fig.10). Since it is a redundant system, although it is mentioned that this mechanism leads to mass reduction, mass and inertia of motors are not considered and three motors were used to provide two DoFs. Also, the design for higher DoFs is far from trivial.

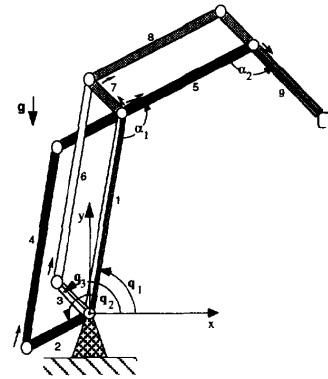


Fig. 10. 9 link 3 DoF redundant parallel manipulator

In another study [31], Lee presents a method to obtain globally optimal motion with the minimal base reaction for redundant mechanical manipulator in his work. The work reduces the formulation of the problem of finding an optimal motion to an optimization problem. However, this paper tries to get the best possible result from an ordinary 3R serial mechanism. The same control concept could be helpful with better (balanced) mechanisms. Some studies have utilized serial wrist with prescribed rotation velocities attached to the mechanism to cancel the shaking moment. [16], [25], [26]. For instance, to dynamically balance the PAMINSA manipulator, [25] (Fig.11) the authors rotate the end effector to provide the

counter-rotation to balance the manipulator’s shaking moment. However, it is not clear from the paper if this could be viable in practical industrial situations when the end effector has to carry a payload or move in a restricted workspace. Researchers

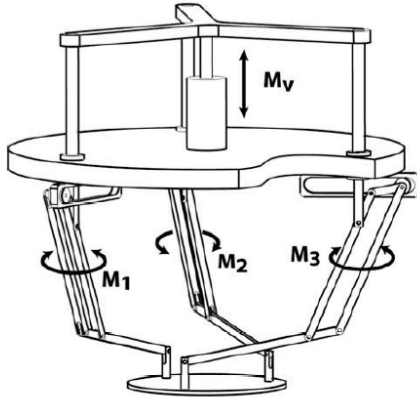


Fig. 11. 4 DoF PAMINSA manipulator, the figure shows the 3 actuated legs and one translational actuation provided at the top. The 3 DoF end effector used to balance the moment is not shown in the simplified diagram

have also added active balancing units to the main mechanism that move in the counter direction to cancel the forces and moments acting on the base [21]–[23]. This method is outside the scope of inherent balancing but could be helpful if stringent weight constraints are not present.

D. Leg by Leg Approach

The approach of dynamically balancing mechanism leg by leg is applicable to parallel architecture platforms. In these platforms, each leg is dynamically balanced and then combined to form a higher DoF dynamically balanced structure. The parallel architecture allows the division of total load between the legs such that it can carry a higher payload and also provide higher stiffness compared to serial manipulators. One of the highly cited papers is the PAMINSA robot [27] (Fig.11) discussed in the previous section. It uses pantograph linkages such that the motion in the vertical and horizontal directions are decoupled. Counter masses are added to balance the shaking force and the end effector is controlled to balance the shaking moment. As discussed in the previous section, the shaking moment is balanced by controlling the velocity of the end effector which is not a practical operation. From the same research group, they presented the Pantopteron-4 which is similar to PAMINSA but has 3 orthogonal translational DoF. Gosselin’s group which developed the balanced 4 bar balanced mechanisms, used the 4 bar mechanisms as elementary links in the development of balanced legs. One such work involved the use of an inverted reactionless 4 bar mechanism, two of which were combined to form a 2 DoF leg [28]. Further, three of these legs were combined to form a 3 DoF parallel mechanism. (Fig.12) In another work, they employed the same inverted 4 bar mechanism but this time they joined them

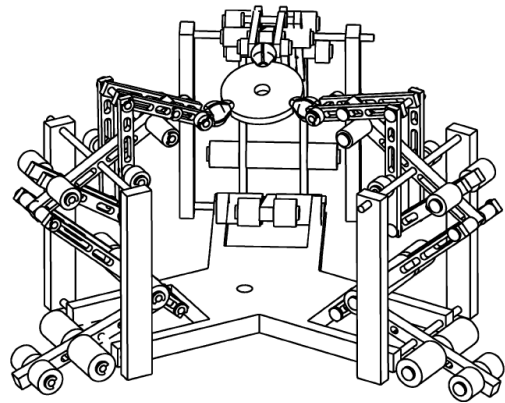


Fig. 12. Prototype of the spatial 3 DoF balanced chain formed by connecting 3 2 DoF legs together with a thin platform

perpendicularly such that 2 DoFs were non-co-planar [9]. These spatial legs were then combined to form a 6 DoFs parallel mechanism. However, no experimental validation was done and the dynamic performance was evaluated by simulating of multi-body dynamics software ADAMS. Also, as previously mentioned, the platform was assumed to have zero thickness. If the platform has non-zero thickness it has to be replaced by 4 equivalent points that are non-co-planar, which then needs 4 legs, further making the design more complex and heavy. The group also developed a 3 DoF spatial parallelepiped mechanism using fundamental balancing principals [29] (Fig.13). This mechanism involved the use of

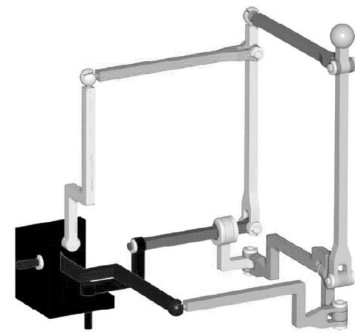


Fig. 13. CAD model of the 3 DoF parallelepiped mechanism

counter-masses and counter-rotations so it was not inherently balanced. Despite not being inherently balanced the unique design of the mechanism allowed for the formulation of an optimization problem so that the geometric center could be brought closer to the CoM such that the counter masses could be made smaller. They also developed a spatial 6 DoF mechanism using the 3 DoF parallelepiped as one of the legs and verified the performance using ADAMS simulations. Despite its optimal design the mechanism developed was still very big and needed 9 counter rotations even though being a 6 DoFs mechanism.

III. METHODS COMPARISON

In this section, the various advantages and disadvantages of the found methods in the literature review are summarized and compared.

The method of principal vectors leads to shaking force balanced mechanisms using vectors graphically. This gives an intuitive understanding of the dynamics of the mechanism. The derivation of the balanced solutions is relatively shorter than the ones using the direct method using the linear and angular momentum equations. Deriving the balanced moment conditions between relative DoF when the relations between their angular velocities become non-linear becomes complex, but it is possible to balance moments as shown in the development of balanced 4 bar mechanisms. One of the other limitations of this method is that they are change point mechanisms [31]. When the links become colinear, the change point state is reached such that the mechanism's motion is not uniquely determined. The parallelogram can switch to anti-parallelogram configurations and then force balance would not be maintained.

Development of mechanisms using the shaking force and moment balanced four-bar mechanism leads to very straightforward development. The development though simple is restricted in the sense that only a limited number of mechanisms can be developed. If there were more balanced mechanisms as elementary pieces then more variety of mechanisms could be possible. Although not too restrictive, the condition that the CoM should lie on the link axis is a limiting factor. It can also be seen from the examples presented in the previous section that the mechanisms become very complex very quickly as the number of DoFs is increased. Also, with parallel mechanisms with a platform, extra legs are needed if the platform is not considered slender to maintain a balanced condition. The algebraic method derived for the four-bar mechanism provides a complete solution set and this method can be utilized in the development of many other balanced mechanisms. Although complete, this method is highly non-intuitive to understand and little dynamic insight could be derived from the algebraic method.

Once the shaking force is balanced, multi DoF systems can be moment balanced by restricting one or more DoFs. This method does not add a lot of mass to the mechanism as this can be achieved using simple elements like a slider. Another way is to make the inertia tensor constant analytically, for this symmetry is sought. In making the design symmetric the designer is constrained to balance conditions after the kinematic synthesis. The optimal way would be to choose a path and then design an inherently balanced mechanism around it. Reactionless path planning is another method employed in redundant manipulators to achieve balanced moment conditions. It has the capacity of kinematical "self-motion" in configuration space, which helps in overcoming an obstacle, joint limit, and singularity configuration avoidance when the manipulator implements some manipulation tasks simultaneously. One exceptional benefit of this method is that

they have a complete workspace with all the DoFs available when the balanced conditions are not needed but can be made reactionless by limiting the workspace. The number of reactionless paths can also be increased by increasing the redundancy in the system. Over-actuation has also shown to be a good alternative when kinematic redundancy is difficult. However, the control is challenging as the force and speed control has to be considered simultaneously.

The leg by leg method is an umbrella term used for all the methods where an open serial chain is balanced and then combined with other similar chains to create a fully balanced parallel structure. Apart from previously mentioned methods this approach considers the complete leg dynamics as a whole and reaches a solution using fundamental momentum equations. The parallel mechanism also allows for higher stiffness and therefore more payload. However, compared to serial architecture parallel architecture is heavier and suffers from many types of singularities. The solutions that are obtained to get balanced conditions are limited and have a risk to have more balance elements than necessary. This happens since individually the legs have more DoFs than the manipulator they are part of. Also, deriving balanced conditions become more difficult if the stage is not considered slender. The non-slender stage also requires 4 legs since the condition becomes non-planar. To compare all the methods presented in the report in a single place a table is created and presented in the appendix. This table ranks the methods based on different criteria and lists out the advantages and disadvantages. The best method can be selected based on the use case.

To sum it up, it can be seen that employing any of the methods leads to substantial weight increase which could be detrimental to the performance especially in cases where weight is a constraint. There are trade-offs when comparing each method and so the method selection choice should be made judiciously. For instance, if weight is a big factor method of balanced four-bar would not be a wise choice but the method of principal vectors could lead to lighter solutions without restrictions on the kinematic design. Similarly, when the mechanism has to be powered with a battery, like on a drone, it would not be wise to use too many motors or use a high-mass system. This would mean that a redundant system or over actuation would not be a wise choice, in this case fully actuated systems like the parallel leg by leg approach could be more helpful. Though not explored in the report it has been observed that sometimes leaving the system partially unbalanced and managing the stability using control methods is also viable. For instance, adaptive control techniques have been shown to be very effective for systems when the full dynamic model is available [33]–[35]. The unbalanced forces and moments are balanced by almost real-time control of propeller speeds. This approach is outside the mechanisms design field but should be known while designing so that the designer can get the best of both worlds.

IV. CONCLUSION

In this report, various methods of inherent dynamic balance were discussed. Dynamic balancing is done to reduce the reaction forces and moments at the base. Fundamental equations leading to dynamic balance conditions were first presented and then four methods to dynamically balance a mechanism were elaborated. Later the methods were compared on various criteria and it was found that there were trade-offs with each method. The best solution would depend on the problem at hand. It was also noted that in some cases full dynamic balancing would not be required and some techniques like adaptive control could be better. It is envisioned that the mechanisms can be made faster and lighter by making use of both design and control concepts.

ACKNOWLEDGMENT

The author would like to thank Volkert Van der Wijk for his constant support during the literature survey.

REFERENCES

- [1] Wu, Yangnian, and Clément M. Gosselin. "Synthesis of reactionless spatial 3-dof and 6-dof mechanisms without separate counter-rotations." *The International Journal of Robotics Research* 23.6 (2004): 625-642.
- [2] Lowen, G. G., and R. S. Berkof. "Survey of investigations into the balancing of linkages." *Journal of mechanisms* 3.4 (1968): 221-231.
- [3] Arakelian, Vigen, and Sébastien Briot. *Balancing of linkages and robot manipulators: advanced methods with illustrative examples*. Vol. 27. Springer, 2015.
- [4] Wei, Bin, and Dan Zhang. "A review of dynamic balancing for robotic mechanisms." *Robotica* 39.1 (2021): 55-71.
- [5] Van der Wijk, V. "Methodology for analysis and synthesis of inherently force and moment-balanced mechanisms." (2014).
- [6] Y. Yorozu, M. Hirano, K. Oka, and Y. Tagawa, "Electron spectroscopy studies on magneto-optical media and plastic substrate interface," *IEEE Transl. J. Magn. Japan*, vol. 2, pp. 740-741, August 1987 [Digests 9th Annual Conf. Magnetics Japan, p. 301, 1982].
- [7] M. Young, *The Technical Writer's Handbook*. Mill Valley, CA: University Science, 1989.
- [8] Meriam, James L., L. Glenn Kraige, and Jeff N. Bolton. *Engineering mechanics: dynamics*. John Wiley and Sons, 2020.
- [9] Wu, Yangnian, and Clément Gosselin. "Design of reactionless 3-DOF and 6-DOF parallel manipulators using parallelepiped mechanisms." *IEEE Transactions on Robotics* 21.5 (2005): 821-833.
- [10] van der Wijk, Volkert, and Just L. Herder. "The work of Otto Fischer and the historical development of his method of principal vectors for mechanism and machine science." *Explorations in the History of Machines and Mechanisms*. Springer, Dordrecht, 2012. 521-534.
- [11] Agrawal, Sunil K., Glenn Gardner, and Stephen Pledgie. "Design and fabrication of an active gravity balanced planar mechanism using auxiliary parallelograms." *J. Mech. Des.* 123.4 (2001): 525-528.
- [12] Gökçe, Ali, and Sunil K. Agrawal. "Mass center of planar mechanisms using auxiliary parallelograms." *International Design Engineering Technical Conferences and Computers and Information in Engineering Conference*. Vol. 80319. American Society of Mechanical Engineers, 1998.
- [13] Agrawal, Sunil K., and Abbas Fattah. "Reactionless space and ground robots: novel designs and concept studies." *Mechanism and Machine theory* 39.1 (2004): 25-40.
- [14] Agrawal, Sunil K., and Abbas Fattah. "Gravity-balancing of spatial robotic manipulators." *Mechanism and machine theory* 39.12 (2004): 1331-1344.
- [15] Fattah, Abbas, and Sunil K. Agrawal. "Design and simulation of a class of spatial reactionless manipulators." *Robotica* 23.1 (2005): 75-81.
- [16] Fattah, Abbas, and Sunil K. Agrawal. "On the design of reactionless 3-DOF planar parallel mechanisms." *Mechanism and Machine theory* 41.1 (2006): 70-82.
- [17] Wei, Bin, and Dan Zhang. "A review of dynamic balancing for robotic mechanisms." *Robotica* 39.1 (2021): 55-71.
- [18] Ricard, Rémi, and Clément M. Gosselin. "On the development of reactionless parallel manipulators." *International Design Engineering Technical Conferences and Computers and Information in Engineering Conference*. Vol. 35173. American Society of Mechanical Engineers, 2000.
- [19] Gosselin, Clément M., et al. "Synthesis and design of reactionless three-degree-of-freedom parallel mechanisms." *IEEE Transactions on Robotics and Automation* 20.2 (2004): 191-199.
- [20] Moore, Brian, Josef Schicho, and Clément M. Gosselin. "Determination of the complete set of shaking force and shaking moment balanced planar four-bar linkages." *Mechanism and Machine theory* 44.7 (2009): 1338-1347.
- [21] van der Wijk, Volkert, and Just L. Herder. "Active dynamic balancing unit for controlled shaking force and shaking moment balancing." *International Design Engineering Technical Conferences and Computers and Information in Engineering Conference*. Vol. 44106. 2010.
- [22] Dresig, H., and Nguyen Phong Dien. "Complete shaking force and shaking moment balancing of mechanisms using a moving rigid body." *Technische Mechanik-European Journal of Engineering Mechanics* 31.2 (2011): 121-131.
- [23] Wang, Kun, et al. "Dynamics analysis of a three-DOF planar serial-parallel mechanism for active dynamic balancing with respect to a given trajectory." *International Journal of Advanced Robotic Systems* 10.1 (2013): 23.
- [24] Papadopoulos, Evangelos, and Ahmed Abu-Abed. "Design and motion planning for a zero-reaction manipulator." *Proceedings of the 1994 IEEE International Conference on Robotics and Automation*. IEEE, 1994.
- [25] Briot, Sébastien, and Vigen Arakelian. "Complete shaking force and shaking moment balancing of the position-orientation decoupled PAMINSA manipulator." In *2009 IEEE/ASME International Conference on Advanced Intelligent Mechatronics*, pp. 1521-1526. IEEE, 2009.
- [26] Arakelian, Vigen, and Sébastien Briot. "Dynamic balancing of the SCARA robot." *17th CISM-IFTOMM Symposium on Robot Design, Dynamics, and Control (RoManSy 2008)*. 2008.
- [27] Briot, Sébastien, Vigen Arakelian, and Sylvain Guégan. "PAMINSA: A new family of partially decoupled parallel manipulators." *Mechanism and Machine Theory* 44.2 (2009): 425-444.
- [28] Gosselin, Clément M., et al. "Synthesis and design of reactionless three-degree-of-freedom parallel mechanisms." *IEEE Transactions on Robotics and Automation* 20.2 (2004): 191-199.
- [29] Wu, Yangnian, and Clément Gosselin. "Design of reactionless 3-DOF and 6-DOF parallel manipulators using parallelepiped mechanisms." *IEEE Transactions on Robotics* 21.5 (2005): 821-833.
- [30] Van Der Wijk, Volkert, et al. "Design and experimental evaluation of a dynamically balanced redundant planar 4-RRR parallel manipulator." *The International Journal of Robotics Research* 32.6 (2013): 744-759.
- [31] Lee, H. P. "Motions with minimal base reactions for redundant manipulators." *Computers and structures* 61.4 (1996): 651-656.
- [32] Chang, Wen-Tung, Chen-Chou Lin, and Long-Long Wu. "A note on Grashof's theorem." *Journal of Marine Science and Technology* 13.4 (2005): 239-248.
- [33] Hanover, Drew, et al. "Performance, Precision, and Payloads: Adaptive Nonlinear MPC for Quadrotors." *arXiv preprint arXiv:2109.04210* (2021).
- [34] Bazylev, Dmitry, et al. "Adaptive control system for quadrotor equipped with robotic arm." *2014 19th international conference on methods and models in automation and robotics (MMAR)*. IEEE, 2014.
- [35] Caccavale, Fabrizio, et al. "Adaptive control for UAVs equipped with a robotic arm." *IFAC Proceedings Volumes* 47.3 (2014): 11049-11054.

APPENDIX A

COMPARISON CHART

In the table shown below the advantages and disadvantages of all the methods considered are tabulated. The table also ranks the methods based on certain criteria. The link by link method that was not discussed in the paper, since it is not inherent balancing, involves addition of extra elements so that each link is balanced individually, starting from the outermost link first.

	Principal Vectors/Auxiliary Parallelogram	Reactionless Path planning(constraint Multi DoF)	Balanced Four Bar	Leg by Leg	Link by Link
Advantages	inightful (follows similarity). Counter rotations are not needed. Overall weight is less compared to addign extra elements	System weight is less with no additional components. Redundancy can be reduced by adding more joints.	Counter rotations are not needed, overall weight is less compared to link by link balancing	Usually a parallel mechanism where the total load is divided btr the legs, higher stiffness and more payload	Simple method to implement, Relevant research very mature
Disadvantages	Change pt mechanisms, sometimes link overlap, singularity, Use of slender links is assumed in the first paper	The optimization methods involved in deriving the best paths are sometimes not insightful, end effector trajectory	Platform is assumed to be very thin so reactionless conditions not practical. The con bar to lie on the link axis to be balanced. Design become too complex for high dof with dynamic with kinematic and dynamic modeling becoming too complex.	Singularity with parallel mechanisms. Limited workspace compared to serial chains	Heavily(150 times as found in the Goszalin paper(2005)
Comments	Moment Balance is based on simtrically designing the mechanism.Use of passive joints makes the moment 0 along one of the directions	Redundant manipulators are used, as you increase the redundancy the possible trajectories increases, overactuation is not equal to kinematic redundancy	If the platform is not slender 4 legs have to used to compensate for out of plane com	The legs in PAMINSA were decoupled first and then balanced	One of the most researched way to balance mechanisms
Examples	[5],[10]-[16]	[16],[24]-[26]	[1],[19]-[20]	[27]-[30]	Not explored in the report, interested readers can refer to [4]
Accuracy	1	1	1	1	1
Weight*	1	2	4	2	4
Power Requirement(Motor)*	1	4	2	2	2
Complexity(Design- High DoF)	3	1	3	2	2
Complexity(Control)	1	4	1	3	1
Moment Balanced	4	1	1	1	3
Support auxially elements(1 least)	4	2	1	2	3
Workspace	2	4	1	2	1

(*)- important factors for a Groue

Fig. 14. Comparison Chart.

3

ADAPT: A 3 Degree of Freedom Reconfigurable Force Balanced Parallel Manipulator for Aerial Applications

ADAPT: A 3 Degree of Freedom Reconfigurable Force Balanced Parallel Manipulator for Aerial Applications

Kartik Suryavanshi¹, Salua Hamaza², Volkert van der Wijk¹ and Just Herder¹

Abstract—In this paper, we present the ADAPT, a novel reconfigurable force-balanced parallel manipulator with pantograph legs for spatial motions applied underneath a drone. The reconfigurable aspect allows different motion-based 3-DoF operation modes like translational, rotational, mixed, planar without disassembly. For the purpose of this study, the manipulator is used in translation mode only. A kinematic model is developed and validated for the manipulator. The design and motion capabilities are also validated both by conducting dynamics simulations of a simplified model on MSC ADAMS, and experiments on the physical setup.

The force-balanced nature of this novel design decouples the motion of the manipulator’s end-effector from the base, zeroing the reaction forces, making this design ideally suited for aerial manipulation in unmanned aerial vehicles (UAVs) applications, or generic floating-base applications.

Index Terms—reactionless force balancing, configurable robot, mechanism design, parallel robot, aerial manipulation

I. INTRODUCTION

In recent years, there has been increasing interest and effort toward the development of Unmanned Aerial Vehicles (UAVs) with manipulation capabilities to be used for civilian purposes. The energy sector has heavily funded research for the development of UAVs that can monitor and inspect physical infrastructure, respond to natural disasters and help with smart cropping for higher yields in the agricultural and meteorological domains [1]. In the EU, several projects with large consortia further developed mechatronic and software solutions to advance the field of aerial manipulation for industrial inspection and maintenance (I&M). To do this, the UAV has to not only do contact-less tasks like surveillance, monitoring, and remote sensing, but also it has to do active tasks like grasping and manipulation [3].

Interest in aerial manipulation has been steadily growing to their exceptional capabilities when combining the versatility of aerial platforms and the manipulation capabilities of robotic arms. However, there are still many research problems to be solved before aerial manipulators can be put to use. One of the major problems is the complex control of the combination of a drone and a manipulator. There are two ways to develop the motion controller for the combined system [4].

¹ These authors are with the Department of Precision and Microsystems Engineering, Faculty of 3ME, TU Delft, the Netherlands. Corresponding author: k.suryavanshi@student.tudelft.nl

² This author is with the Department of Control Operations, Faculty of Aerospace Engineering, TU Delft, the Netherlands.

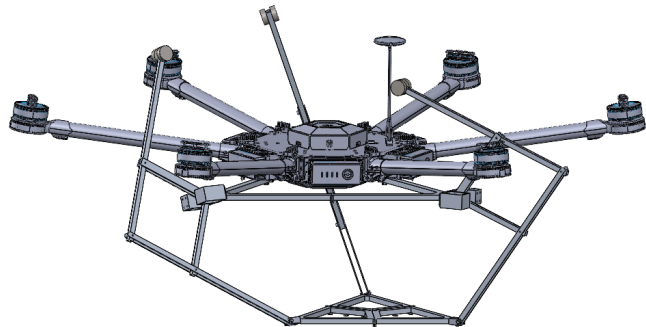


Fig. 1. CAD of the drone with the force-balanced manipulator.

The first approach is to consider the manipulators and the aerial vehicle as two separate entities which have to be controlled independently, i.e. *decentralised* approach. Generally, the manipulators in this approach are considered to be very lightweight and relatively underactuated, such that they do not have a great impact on the dynamics of the aerial vehicle [5]. The decentralised approach is popular in the aerial robotics community, it allows a faster implementation on the two subsystems through decoupling, omitting the need for a full multi-body dynamic model. However, this approach fails when the motion becomes too demanding in terms of accelerations involved, resulting in large tracking errors.

The second approach is to create a dynamic model, such that the UAV and manipulator combination become a single entity [6]. The inertia matrix in this approach consists of coupling terms such that the manipulator and aircraft both affect each other. Having a complete coupled dynamic model leads to the system having better performance in terms of positioning and stability. However, since the system relies on a complete dynamic model, the controller becomes rather complex [7]–[9]. Secondly, model-based controllers assume that torque feedback at the actuator is available, however this is not always the case, especially on lightweight manipulators.

Extensive research in aerial manipulation is conducted in making the controllers better. Conversely, not a lot of thought has been put into improving the manipulator mechanical design such that the dynamical model itself becomes simpler. Removing the coupling between the two subsystems can ease the controller, as the UAV only perceives the manipulator as an additional static mass that does not affect the aircraft’s

dynamics.

In this paper, we propose a new balanced manipulator that does not create any reaction forces during its motion throughout its configuration space. This force-balanced design is such that the center of mass of the manipulator remains fixed. Therefore, there are no coupling mass terms in the complete inertia matrix in the dynamic model of the complete system. This design would make the controller much simpler such that the aerial vehicle still manages to do highly dynamic maneuvers, even with an integrated manipulator.

The paper is organized as follows. In Section 2 the manipulator design and balance conditions are presented. Section 3 discusses the kinematics of the design manipulator. This is followed by a brief analysis of the singularities in Section 4. In Section 5 the workspace volume is calculated using geometric methods. Section 6 presents the simulations conducted on multibody simulation software MSC ADAMS. In Section 7 the experimental setup is presented followed by experiments in Section 8, a discussion in Section 9, and finally conclusion in Section 10.

II. MANIPULATOR DESIGN

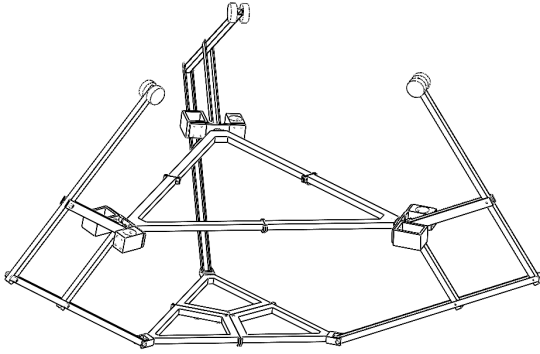


Fig. 2. Wire-frame model of the three legged forced balanced manipulator. Each leg is composed of an inherently forced balanced pantograph mechanism

One way to create force balance spatial manipulators is by designing a structure composed of spatial force-balanced elements as legs such that there is spatial force balancing in individual legs themselves as well as the whole mechanism. This leads to heavier leg designs as a spatially balanced leg requires more balancing elements involving a more complex structure [10]. Another way to create a balanced mechanism is to take 2D planar force-balanced elements and combine them to create a spatial 3D mechanism. The legs are combined in such a way that the addition of moment/force constraint wrenches span the full three dimensions. In other words, the moment/force constraints should be independent such that they form a basis in three dimensions. The latter method is used to create a spatially force-balanced mechanism in this work since it leads to a design that uses fewer elements for balancing and is less complex.

This spatial forced balanced mechanism is designed in a manner such that it is composed of the pantograph as its legs.

A pantograph is a 2-DoF mechanism that is symmetric about the center point 'S' as shown in the Fig.4 (For details on the naming paradigm of various elements of the pantograph in this paper, the reader is suggested the work of Van der Wijk [10]). This symmetry allows the construction of mass symmetric mechanisms which is a precursor to force-balanced mechanisms. The constraint imposed by each leg is such that the constraint wrench is a pure moment, reciprocal to all the R joints. The moment constraint wrench is such that it spans the 3D space consequently allowing translation in 3D space for the platform. The three constraints would remain independent unless they reach singularity as defined in Section IV.

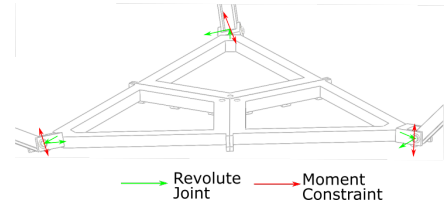


Fig. 3. The constraint wrench in a parallel manipulator is the sum of all the constraint from all the legs. The constraint moment from an individual leg is perpendicular to all the revolute joints. The revolute joints are shown in green colour and constraint moments in red. The sum of these moment constraints span the full 3D space such that the reciprocal freedom screw shows all three translations for the platform.

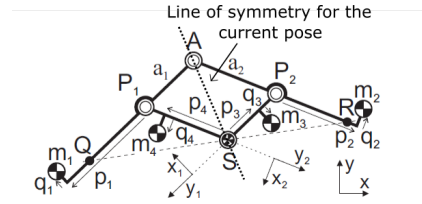


Fig. 4. General 2-DoF pantograph structure with the centre of mass of the structure at point S. The pantograph is mass symmetric about the instantaneous line joining points A and S. Since the legs are mass symmetric therefore the q's have a value of zero and the pantograph can further be simplified as shown in one of the legs in Fig. 5(b). Details on various parameters and motion capabilities of a pantograph can be found in Wijk's work. [10]

Van der Wijk formulated the force balance conditions for pantographs using the linear momentum equations which have been reproduced here. First, one of the DoFs in the pantograph (Fig.4) is fixed such that the link P_1A is solely in rotation and the link P_2A is solely in translation in the figure. The linear momentum is then written with the y-axis aligned in the SP_2 direction. For the overall CoM to be fixed in its position, the linear momentum should be zero.

$$\overline{L}_1 = \begin{bmatrix} -m_1p_1 + m_2a_1 + m_3p_3 \\ m_1q_1 - m_3q_3 \end{bmatrix} \dot{\theta}_1 = \begin{bmatrix} 0 \\ 0 \end{bmatrix} \quad (1)$$

Similar to the first DoF, the second DoF's linear momentum can be written in the same manner and equated to zero.

$$\overline{L}_2 = \begin{bmatrix} -m_2p_2 + m_1a_2 + m_4p_4 \\ m_2q_2 - m_4q_4 \end{bmatrix} \dot{\theta}_2 = \begin{bmatrix} 0 \\ 0 \end{bmatrix} \quad (2)$$

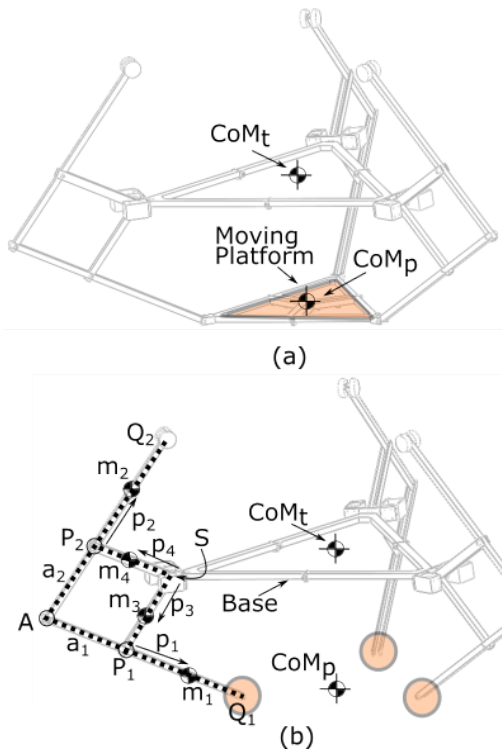


Fig. 5. (a) The manipulator with the platform mass equivalent to the mass of the three m_2 (Fig 4) masses. (b) Platform replaced with three-point masses at the legs in the equivalent model. The base center of mass, CoM_t , is invariant for all the motions. The equivalent model helps in decoupling of legs which allows fulfilling the balance conditions Eq 4 per individual leg. The tri-symmetric design allows the center of mass of the platform CoM_p to be in the same position in the equivalent model as it were in the actual model.

Combining the two equations (Eq.1 and Eq.2) we get the following four conditions for a pantograph to have its CoM fixed at S and therefore be forced balanced at S .

$$\begin{aligned}
 m_1 p_1 &= m_2 a_1 + m_3 p_3 \\
 m_1 q_1 &= m_3 q_3 \\
 m_2 p_2 &= m_1 a_2 + m_4 p_4 \\
 m_2 q_2 &= m_4 q_4
 \end{aligned} \tag{3}$$

Since the legs are mass symmetric, the values of all the q 's become zero and therefore only two equations need to be solved.

$$\begin{aligned}
 m_1 p_1 &= m_2 a_1 + m_3 p_3 \\
 m_2 p_2 &= m_1 a_2 + m_4 p_4
 \end{aligned} \tag{4}$$

The novel architecture of ADAPT is generated by creating 3 intersecting planes for the robot's legs, equispaced at 120° . On each plane lays a pantograph mechanism. The overall CoM of the assembly is depicted as CoM_t in Fig. 5(a) - this point also remains invariant for any motion of the platform. The invariant CoMs (S s) of the three pantographs are joined together to the fixed base via universal joints. The lower half of the pantographs (SP_1Q_1) are joined together to a moving platform

via 3 universal joints spaced at 120 degrees. The upper half of the pantographs (SP_2Q_2) is free to move. Combining the legs in this way makes the manipulator force balanced. This can be seen by dividing the platform mass equally between the three legs such that each leg is a simple force-balanced pantograph (Fig. 5)

The assembly like such makes the lower half of the setup similar to the Double Y 3-5R parallel mechanism (DYMO) presented by Zlatanov et. al. [17]

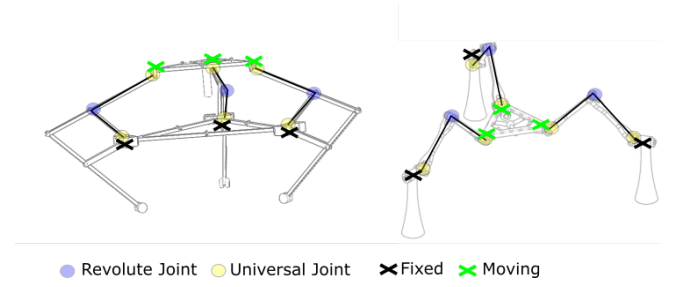


Fig. 6. The similarity between the current manipulator (left) and the DYMO manipulator. It can be seen that the bottom portion of the current manipulator is kinematically exactly similar to the DYMO manipulator.

The DYMO robot has five fundamentally different operation modes: translation, rotation, mixed (rotation+ translation), planar, and no motion at all. The translation mode is utilized in the current work to find a forced balanced alternative to the Delta robot. This was done since the Delta robot motion capabilities are predominantly exploited for various applications. While the mechanism is supposed to only translate, the mechanism can also show mixed motions under certain circumstances that are discussed later when singularities are introduced in the Section IV.

III. KINEMATICS

A. Forward Kinematics

ADAPT consists of a fixed base connected to a moving platform (end-effector) by three parallel kinematic chains as its legs, as depicted in Fig. 7. Each leg has several passive joints and one active joint centred at each pantograph's CoM, placed symmetrically with respect to the pantograph's legs. This design makes the ADAPT robot different from conventional parallel manipulators where the active joint features as the first joint, at the base. The motion in ADAPT is transmitted to the moving platform by the lower portion of the pantograph (SP_1Q_1). Moreover, unlike a generic Delta robot, the intermediate leg joint is a revolute and not a universal. There is a 2-DoF relative motion within the Delta robot's leg, contrasting with the 1-DoF relative motion in ADAPT. The schematic in Fig.7 shows the kinematic parameters of one of the legs where we just consider the lower portion of the pantograph. The motion of the upper portion (SP_2Q_2), Fig. 5) of the leg is symmetric to the motion of the lower portion.

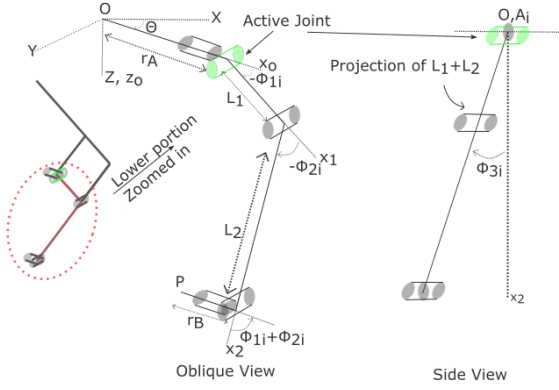


Fig. 7. Schematic diagram of the lower portion of one of the legs with the kinematic parameters. The ϕ_{3i} angle rotates the full leg (Side View) unlike the Delta robot where only the upper link of the leg moves relative to the lower leg. There is 2DoF relative motion within a Delta robot leg contrasting with the 1DoF relative motion in the current leg.

O represents the center of the fixed platform, while P is the center of the moving platform. The first Cartesian coordinate frame is XYZ which is fixed to the point O . The next reference frame is $X_o Y_o Z_o$ which has the same XY plane but the frame is rotated about the Z -axis by angle θ_i , which is constant and i is the number of the leg $i=1,2,3$. The frame $X_o Y_o Z_o$ has its X -axis towards the attachment point of the leg. r_A and r_B are the radii of the two platforms. Each leg is intended to constrain one rotation such that the platform is only allowed translations when the three legs are attached. So the moving platform is always horizontal. The first revolute joint (the passive joint next to point O is the first joint, the active joint is the second joint, and so on) rotates the complete leg about its X -axis. This angle is denoted by ϕ_{3i} . The angle

between the first link and the base is denoted by ϕ_{1i} . The angle between the first link and the second link is denoted by ϕ_{2i} . Since the platform is constrained to remain horizontal the magnitude of the fourth angle (fourth revolute from the top) is equal to the sum of the magnitudes of the second and the third angles but with a negative sign. This implicit definition makes kinematics easier to formulate since the number of variables is reduced. Similarly, the magnitude of the last joint angle is equal to and opposite to the magnitude of the first joint angle ($-\phi_{3i}$). L_1 and L_2 are the link lengths as shown in the Fig. 7.

To locate the position of point P of the moving platform Denavit-Hartenberg transformation matrices are defined. The transformation matrices are 4×4 homogeneous matrices with a 3×3 rotation component on the left and a 3×1 position vector on the right of the matrix. Generic three rotation matrices three translation matrices, and the intermediate frame transformation matrices are given in the Appendix. The benefit of homogeneous matrices is that they can be directly multiplied to get the transformation from one frame to the next. For instance, transformation matrix T_{r_z} when multiplied to $T_{t_{r_a}}$ makes the coordinate transformation from the reference frame at the base (XYZ) to the reference frame at the leg attachment point. The intermediate frames have not been represented in the figure for the sake of clarity. The sequence of matrix multiplication results in the transformation from the base frame to the platform frame.

$$T_{r_p} = T_{r_z} T_{t_{r_a}} T_{r_{x_o}} T_{r_{y_o}} T_{t_{L_1}} T_{r_{y_1}} T_{t_{L_2}} T_{r_{y_2}} T_{r_{x_2}} T_{t_{r_b}} T_{r_{z_2}} \quad (5)$$

The resultant matrix is quite large to produce here therefore just the 3×1 matrix from the top right corner has been extracted. This matrix denotes the position of the end effector.

$$\begin{pmatrix} r_A C(\theta_i) - r_B C(\theta_i) + L_1 C(\phi_{11}) C(\theta_i) + L_2 C(\phi_{11}) C(\phi_{21}) C(\theta_i) - L_2 C(\theta_i) S(\phi_{11}) S(\phi_{21}) - L_1 S(\phi_{11}) S(\phi_{21}) S(\theta_i) - L_2 C(\phi_{11}) S(\phi_{21}) S(\theta_i) - L_2 C(\phi_{21}) S(\phi_{11}) S(\phi_{31}) S(\theta_i) \\ r_A S(\theta_i) - r_B S(\theta_i) + L_1 C(\phi_{11}) S(\theta_i) + L_2 C(\phi_{11}) C(\phi_{21}) S(\theta_i) + L_1 C(\theta_i) S(\phi_{11}) S(\phi_{21}) - L_2 S(\phi_{11}) S(\phi_{21}) S(\theta_i) + L_2 C(\phi_{11}) C(\theta_i) S(\phi_{21}) S(\phi_{31}) + L_2 C(\phi_{21}) C(\theta_i) S(\phi_{11}) S(\phi_{31}) \\ C(\phi_{31}) (L_2 S(\phi_{11} + \phi_{21}) + L_1 S(\phi_{11})) \end{pmatrix} \quad (6)$$

Where $S()$ and $C()$ are used for sin and cos functions respectively for brevity. In the complete transformation matrix, the rotation matrix is a constant since for the current use of the manipulator there is no rotation of the platform due to the legs, but there is a constant angle between the leg and the fixed base frame.

B. Inverse Kinematics

Researchers usually find the inverse kinematic relation by considering a loop equation and getting rid of passive joint variables from the kinematic equations using some tricks like taking the scalar product which makes the equations independent of the passive variables such that only the active input variables remain in the equations which are required for the Jacobian [12]–[14]. In the current case, the active revolute joints are ϕ_{1i} ; $i=1,2,3$, and all the rest of the revolute joints

are passive. Since the active joint comes after the passive joint, ϕ_{3i} , the same trick cannot be applied since the velocity equations are still dependent on the passive variables.

The goal of inverse kinematics is to get the angles of the active joints for a specific position of the end effector. We have three equations for the x , y , and z position of the center of the platform which is composed of three variables ϕ_{11} , ϕ_{21} , and ϕ_{31} . Since it is not possible to analytically solve all three equations simultaneously, some reductions are done to get a relation between two variables. These reductions were possible due to the geometrical conditions in the manipulator unlike the analytical reductions in the previous works. It can be seen in the figure that the magnitude of the vector OP does not depend on the passive variable ϕ_{31} . Since the leg is planar, only the planar components matter in its magnitude. We can see this by assuming all the joints to be fixed and varying ϕ_{31}

variable, the magnitude of the vector OP is independent of angle ϕ_{3i} .

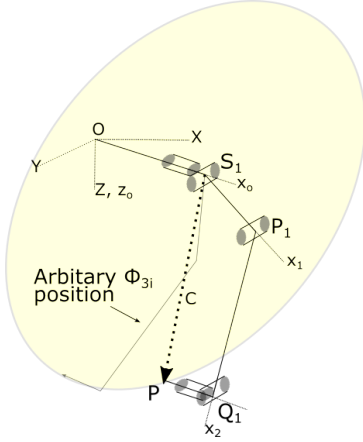


Fig. 8. Schematic diagram of one of the legs with the kinematic parameters. When all the joints are kept fixed and only ϕ_{3i} is allowed to move then the leg endpoint forms a circle with a fixed radius. This radius (C) is independent of the joint variable ϕ_{3i}

Therefore the leg ($S_1P_1Q_1P$ in Fig. 8) forms a circle with radius C as can be seen in the figure in yellow. We can calculate the length of the vector OP by squaring and adding the $x, y,$ and z position equations in the transformation matrix. Doing that we see that the dependence on ϕ_{3i} indeed falls off and we can get a relation between ϕ_{2i} and ϕ_{1i} . We can substitute ϕ_{2i} in the z position equation in the transformation matrix and find a relation between ϕ_{1i} and ϕ_{3i} . We can then substitute the known values of ϕ_{3i} , and ϕ_{2i} in terms of ϕ_{1i} in x position equation to find the value of ϕ_{1i} in terms of the known position variables p_x, p_y and p_z . The results and explanation of each step can be found in the Appendix.

Once the equation is derived in terms of ϕ_{1i} , the Jacobian can be evaluated to find the platform velocity with respect to the time derivative of ϕ_{1i} . These Jacobian matrices are also given in the Appendix. The relation between platform velocity (v) and input velocity ($\dot{\theta}$) can be represented in the following form

$$J_p * v = J_\theta * \dot{\theta} \quad (7)$$

It is found that J_θ is a diagonal matrix which implies that the input velocities are independent of each other when moving the platform, which is similar to a conventional Delta robot. Whereas, J_p is a full matrix indicating that the velocity along all three axes is affected by a single input, again similar to a conventional Delta robot.

IV. SINGULARITIES

Since the manipulator configuration is similar to a Delta robot, it shares some of the same singularities. Motion singularities occur when the jacobian matrices J_θ or J_p become rank deficient [2].

A. Inverse Kinematic Singularities



Fig. 9. CAD model of the current manipulator in its singular conditions. The first figure corresponds to the situation when the legs fold in. The second figure corresponds to the case when the legs are completely stretched out. The third figure corresponds to the situation when the legs are sideways. These in turn define the boundary of the workspace.

Inverse kinematic singularities occur when the determinant of J_θ (Eq (7)) matrix becomes zero. This corresponds to the situations where for any non-zero value of the input angle ϕ_{1i} , there exists platform velocities that cannot be achieved, that is, the motion is zero in certain directions. It is observed that these singularities occur at the extremities which in turn limits the workspace of the manipulator. Typically, these unachievable platform velocities would be orthogonal to the boundary and directed toward the outside of the workspace [2]. For the current manipulator, there are two such cases

- i) $\phi_{2i} = 0$ or $\pi \forall i$, or
- ii) $\phi_{3i} = \pi/2$ or $-\pi/2 \forall i$

The first situation is the case when the first link of a leg is parallel or anti-parallel to the second leg. This corresponds to the case when the manipulator is fully contracted or extended as shown in the Fig. 9. The second situation arises when one of the legs is fully laid on its side such that the leg lies completely in the XY plane. This also determines the workspace boundary on the side. The reader has to note that these conditions are theoretically defined, the actual extremities would be different since the joints have mechanical limits and the links have some physical dimensions.

B. Forward Kinematic Singularities

Direct kinematic singularities occur when the determinant of the J_p matrix becomes zero. This corresponds to situations when no motion is given at the inputs and there is still a motion at the end effector, generating extra DoF in the system. Finding the direct kinematic singularities is more complicated than the inverse case since the related direct jacobian matrix J_p is not diagonal. Since it is not possible to find the null space of the determinant analytically or numerically [15], simpler robot geometries were looked at with similar configurations to find these singularities intuitively. It can be noticed that the top picture in the Fig. 9 is exactly similar to the planar 3RRR robot. This indicates that it will also share the same singularities.

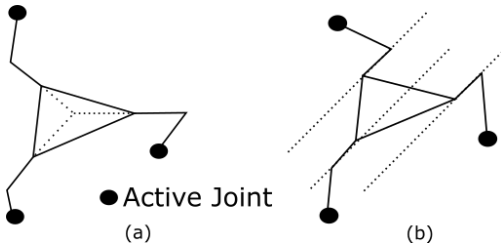


Fig. 10. Schematic drawing of the planar configuration of the current manipulator. (a) Depicts the singularity condition when the legs intersect and (b) depicts singularity when the legs are parallel. In both cases, the legs are not independent and hence gain an extra DoF

For the planar case, the singularities occur when the links joining the platform are oriented such that the constraints do not remain independent anymore Fig.10. This happens when the links joining the platform intersect at one point or they are parallel [18]. Since the research on this configuration is very mature, it is not discussed further in this paper.

C. Constraint singularities

Besides the conventional singularities, since the manipulator is based on the DYMO parallel manipulator, it also suffers from the same constraint singularities. The configuration space of the manipulator is the same as the DYMO robot [1]. The symmetric part is just there for balancing and does not affect the configuration space. Constraint singularities are singular points of the configuration space of the manipulator. These singularities separate different configuration spaces and allow for dramatically different operation modes. One of the operation modes has been exploited in the development of the current manipulator translational capabilities. As suggested in the paper, for the manipulator to remain parallel and work in the translational mode the following singularity conditions should be avoided.

- i) $P \in O_z$; meaning that the platform center is on the z-axis of the base platform.
- ii) Platform plane and the base plane coincide.
- iii) A combination of i) and ii) meaning P and O coincide

Condition (ii) and (iii) cannot occur in the physical robot so they can be overlooked. If in case the manipulator is in the

singularity condition (i), the platform has to remain parallel to the base plane to remain in the translation mode.



Fig. 11. CAD model of the current manipulator transitioning from translation mode to mixed freedom mode. As the center moves away from the center's vertical axis the tilt angle increases.

The platform can leave the translation mode and get into an undesired mixed freedom mode operation through the constraint singularity (Fig.11), that is when the $P \in O_z$ is described in the paper [1]. When this happens the platform still has 3 DoFs but the platform gains the ability to tilt. The tilt angle of the platform is not free but it is determined by the location of the platform and the base centers. The base and the platform centers are along the ray from the origin O and at half the tilt angle from the vertical axis. Therefore, along the vertical axis, the platform tilt is zero. Along a ray inclined 45 degrees, the platform tilt is 90 degrees, and so on. As previously mentioned for the platform to avoid transitioning into mixed operation mode, the platform has to remain horizontal while going through the constraint singularity points. More details on this and other operation modes can be found in the DYMO paper [1].

V. WORKSPACE

Like in the Delta robot, the workspace of the current robot is expected to have some irregularities and dents when the robot configuration is in singularity. Usually, inverse kinematic singularities are found by setting the Jacobian to zero. This determines the limits of the workspace of the manipulator. However, it is not possible to find the null space of the inverse kinematic Jacobian analytically for this kind of a closed parallel structure. [15]. To estimate the workspace, the method suggested in paper [17] was adopted. They define the notion of the Maximum Surrounded Workspace which results in a solid volume. The solid volume of the workspace although crude makes the calculations much easier. The solid volume also helps to visualize the changes in the workspace when parameters are changed facilitating a kinematic-based design. In this method, the planar reach limits on the legs are identified which results in a surface. Since the design is

symmetric this surface is revolved to get the complete volume of the manipulator. Since the goal was to manually optimize the lengths to get the maximum workspace, the drone body was also included to provide geometrical constraints. The manipulator motion is restricted due to interference with the drone body which provided the geometrical constraints. The drone DJI Matrice 600 geometry was selected for workspace optimization since it had among the best flight time for a 2kg payload for a commercial drone. 2kg was chosen as the upper limit of the weight of the full manipulator setup.

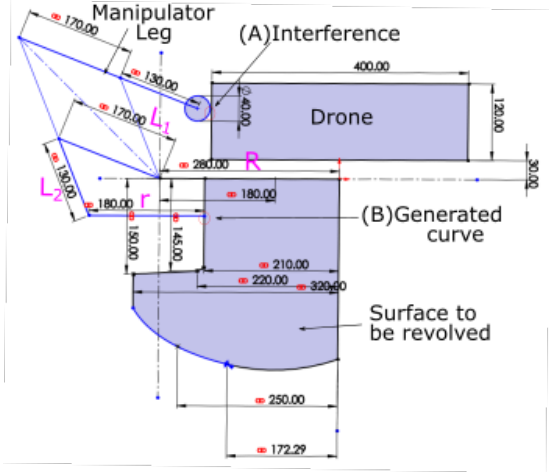


Fig. 12. Planar reach limits of one of the legs. The workspace solid volume can be found by revolving the surface S around the central axis.

As can be seen in Figure with A, the upper part of the pantograph would interfere with the drone body. The interference path of the upper part dictates the path of the center point of the platform which has been manually created (denoted by B). The manually generated path can be revolved around the center line due to the symmetrical nature of the manipulator which gives the workspace volume. Four parameters affect the workspace volume; the radius of the base (R), the length of the first link (l_1), the length of the second link (l_2), and the radius of the platform (r). Since an analytical model with all these parameters could not be formulated, each parameter was varied individually and their effect on the workspace volume was noted. The starting values of the parameters were as follows; $R = 250mm$, $L_1 = 150mm$, $L_2 = 170mm$ and $r = 200mm$. This procedure is elaborated on in the Appendix.

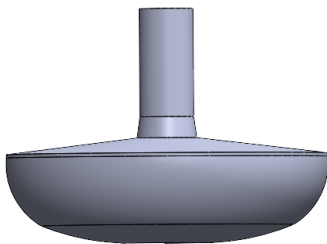


Fig. 13. The workspace shape and volume with the starting values.

It should be noted that the masses of the links were not considered but to have the overall mass of the manipulator within the 2Kg limit the masses of the links have to be kept low. This means that the link lengths cannot be infinitely increased but rather have to be chosen optimally for the highest workspace volume. Considering masses and the workspace the parameters were changed simultaneously such that a computer-assisted manual optimization could be done. With this manual optimization, the following favorable parameter values were found. $R = 280mm$, $L_1 = 170mm$, $L_2 = 130mm$ and $r = 180mm$. The consequent workspace is shown below.



Fig. 14. The computer assisted manually optimized workspace of the forced balanced manipulator

The optimized design has a workspace volume of 3.5 times that of the initial design. Note that, as mentioned previously, this manual method of optimizing the workspace volume does not consider the singularities and other breaks in the volume. This method only guides us to preliminary values that can further be optimized by formulating an analytical model. The values were rounded off to the nearest integer as it also leads to integer values in the balance conditions in Eq. 4. Consequently, it also helped in making the calculation of dimensions of manufactured components easier.

VI. DYNAMIC SIMULATIONS

Dynamic simulations were performed on the multi-body dynamics simulation software MSC ADAMS to validate that the design was forced-balanced. A simplified model of the manipulator was developed for simulation since the simulation attempts on the actual design failed (Fig. 15). The simulation could not run on the actual setup as there were two links for a single leg (for mass symmetry such that the center of mass is in the middle of the two links; giving an over-constraint) that ADAMS could not handle. In the simplified model, the two links were replaced by a single leg such that the geometry and mass values were still conserved. The mass and length values were calculated beforehand in a MATLAB script. These values are given in the Appendix. The leg links were allowed to intersect to give the same motion range to the link as there in the real setup. Since there were still numerical errors in the simplified model, a simple pantograph was simulated to estimate the order of numerical errors and how they cascaded when the system was made bigger. This is shown in the Appendix. Since the numerical errors were smaller in a pantograph, this ushered in the development of a further simplified model also given in the Appendix. The numerical error in the further simplified simulation was in

the same order as in the simplified model. Therefore, the simplified design was deemed sufficient for determining the reaction forces.

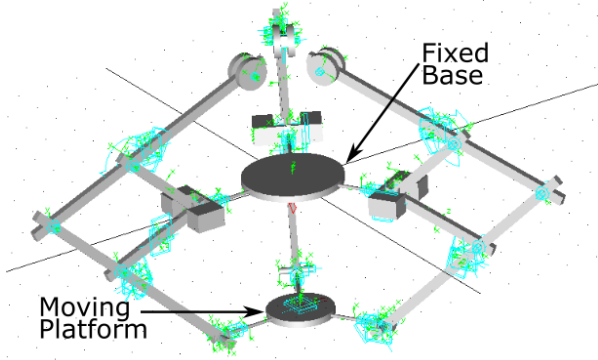


Fig. 15. The simplified model of the manipulator. In this case the joints were simplified and a single link was used in places where there were two to avoid over-constraints..

In simulation, the base is fixed and the platform is allowed to move. Joints are modelled as passive. The reaction forces were evaluated at the fixed base joint in the X and Y directions. A step angular input was given to the first leg to traverse in the X direction and then come back to the origin. As can be seen in the graph (Fig.16) , the reaction forces were in the order of 10^{-5} N. This is due to the errors (Round off error, Discretization error, Truncation error) since the solver simulates the system numerically. The unbalanced case was also simulated. In the unbalanced case, the masses of the counter-masses at the end of the links were made zero, and rest everything was the same.

In the unbalanced case, since the manipulator is not balanced, the platform goes down due to gravity, unlike in the balanced case where it stays put. When the same simulation was run, it was seen that the platform does not remain horizontal and starts to tilt. It can be seen from the results that the forces are significantly higher in the unbalanced case.

A simulation was also conducted to see the force response of the manipulator when a constant force is applied to the moving platform. It could be seen that the applied force of 1N is directly transmitted to the base and there is an exactly equal reaction force in the opposite direction. This is an attribute of a statically balanced mechanism that does not store any potential energy and hence cannot generate any additional forces. The numerical error is still present when the Y direction reaction forces are plotted independently (Fig.18,(Bottom)).

VII. EXPERIMENTAL SETUP

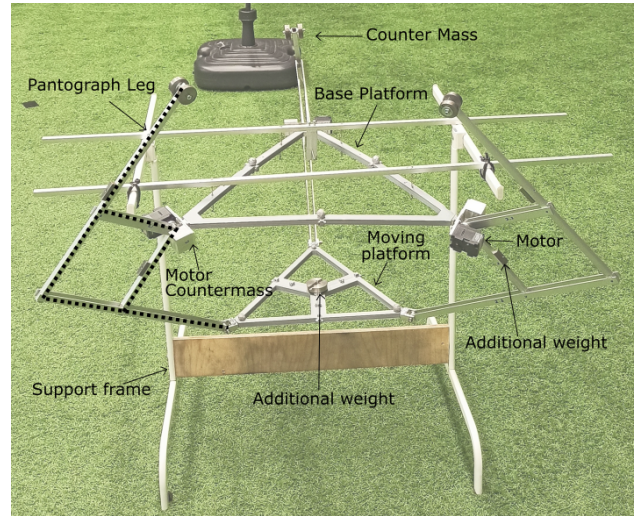


Fig. 19. Experimental Setup of the reactionless manipulator. Additional weight has been added to the links so that the links with equal lengths (but different cross-sections) have equal masses. The additional mass has also been added to the platform so that the total moving mass of the platform is equal to the sum of the masses of the counterweight.

A. Fabrication

The starting point in the fabrication was the selection of motors to drive each of the legs independently. The motor had to just work against friction since the work done in moving links in statically balanced mechanisms is ideally zero, so the smallest possible motors could be chosen. However, the motor was selected such that it could drive an unbalanced leg throughout its range of motion for demonstration purposes. The length and mass of link L_1 (Fig. 7) was chosen to dictate the lengths and masses of the rest of the variables in Eq.4. Since the equations were dependent no optimization was needed once lengths and masses were defined for link L_1 . Standard aluminum plates were used as links and the dimensions were kept as close as possible to the optimized values found in Section V. The length of the link L_1 was chosen to be 170mm which resulted in the mass of 26g with the standard aluminum plate. Consequently, the lengths and masses of the rest of the links were defined. These values can be found in the Appendix. The counter-masses have not been added to the table but they were within the gram order accurate to the masses of the original bodies. Some additional masses have been added to bring the mass of components that have lesser mass closer to the ones formulated through the balance conditions Eq 4 (also equal to the values used in simulations). The masses of those components were not calculated beforehand but were calculated ad-hoc during the manufacturing process. The masses of the generic motors were also included which resulted in the total weight of the setup to be around 1.9Kgs. The torque required to drive an unbalanced leg was simulated in SolidWorks and it was found that Dynamixel XL430-W250-T could be selected. The motor

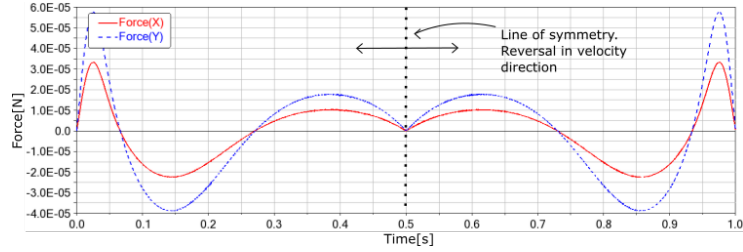


Fig. 16. Reaction forces in the X and the Y direction at the base for straight line traversal of the balanced manipulator platform

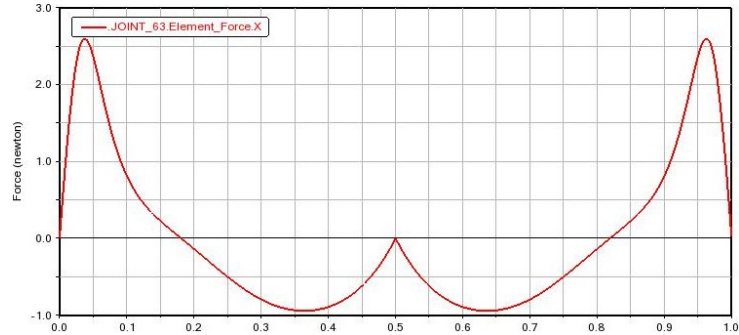


Fig. 17. Reaction forces in the X direction at the base for straight-line traversal of the unbalanced manipulator platform

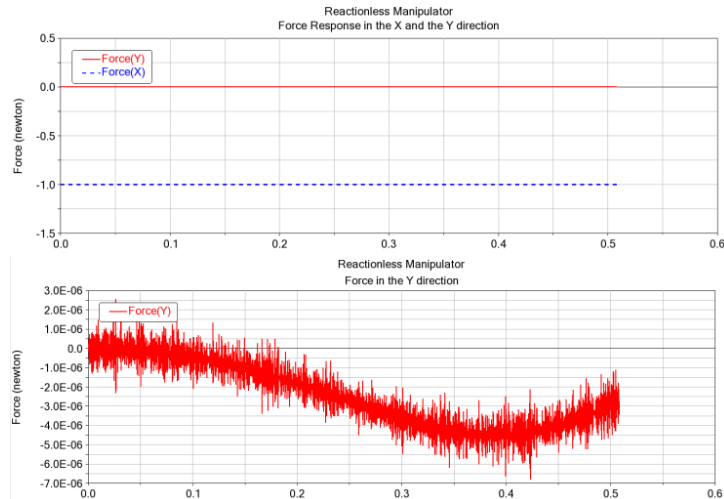


Fig. 18. TOP: Reaction forces X and Y direction at the base of the platform when a force of one newton is applied. Here the numerical errors are not visible as they are relatively very small compared to the actual force value Bottom: Numerical error present as an artifact of the simulation is discernible when the force in the Y direction is plotted independently.

had a stall torque of 1.4 Nm which resulted in a factor of safety close to 3.

The mass of the base does not matter since it is fixed and not part of the pantograph moving geometry. However, the mass of the moving platform matters since it is part of the moving geometry. The platform had to be designed in a manner such that the masses could be equally divided into the three legs yet conserving the original position of the center of mass (Fig. 5). Therefore, a triangular design of the moving platform was selected that was tri-symmetrical which allowed

equivalent division of the platform mass to the three legs. The platform mass was made equal to the sum of the three m2 masses to fulfill the balance conditions Eq 4. Moreover, the additional masses and the mass of m2 were made with steel so they occupy less volumetric space since the geometry did not matter. The condition was that CoM had to lie at the joint center.

B. Electronics and Control

Dynamixel motors come with a fully integrated DC Motor, Controller, Driver, Sensor, and Network all in one servo

model so the auxiliary components required were very less. The motors also come with a range of compatible products which made the development of control circuitry fairly simple. Apart from the motors, Arduino Uno-compatible shields were used with motors, connected in a Daisy chain, which made controlling the motors simultaneously fairly straightforward. An LN-101 was used to serially communicate with the laptop which was used to read the position of all the motors in real-time. Inverse Kinematics was solved off-board in Matlab to get the individual motor angular rotations for various positions. The calculated values were then sent as input to Arduino connected integrated with the shield to the motors running in position mode.

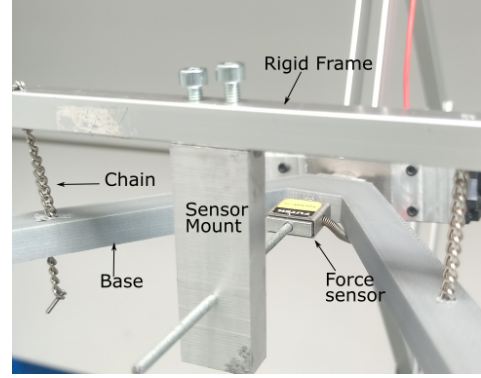


Fig. 20. Experimental setup with the base attached to the frame via four chains.

C. Measurement Setup

The force was measured in the X direction every 100ms using the FUTEK LSB bi-directional load cell. The load cell is connected to the National Instruments Multi-function I/O device which is controlled with a LabVIEW interface. A snippet of a LabView User Interface along with a graphical source code block diagram is given in the Appendix.

VIII. EXPERIMENTS

A. Static balance

For a mechanism to be forced balanced it has to be statically balanced first. To verify this, simple experiments were conducted where the platform was moved to different locations in its workspace and seen if it stayed in its position where it was left. The experiments showed that the manipulator was indeed statically balanced for all the locations in its workspace. The platform stayed statically balanced even in situations when the platform had pitch/yaw/roll angles.

B. Force balance

To check force-balanced conditions the experimental setup was slightly modified. The base was hung to the rigid frame using four chains which allowed the planar motion of the base relative to the frame. The sensor was fixed between the base and the rigid frame (Fig. 20) which measured the reaction force on the base when the platform was moved. Theoretically, it is expected that for any motion of the platform, the reaction at the base should be zero.

1) *Unbalanced:* In the unbalanced case, the counter masses displayed in Fig 26 are removed to emulate the behavior of a generic unbalanced 3-leg parallel manipulator. Doing so with back-drivable motors brings the platform to the least potential energy state at the bottom. Like the simulation, a step input is given to the first leg to traverse in the X direction and then come back to the origin. Unlike the simulation where no damping or stiction was modeled, the stiction in joints in the practical setup made the platform not translate much in the x direction. Rather the platform tilted more and so lower force values around ($\approx .6N$) were recorded (Fig. 21).

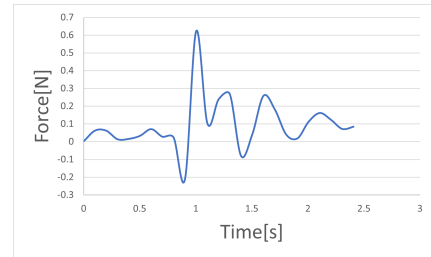


Fig. 21. Reaction forces in the case of an unbalanced manipulator in the X direction for the experiment when the platform is moved forward and back in the X direction. The motion is such $\phi_{11} = 40^\circ$ in the middle of the cycle.

Since the first experiment was not satisfactory a second experiment was conducted. In this experiment, the platform was raised such that, $\phi_{1i} = 40^\circ$. Executing this trajectory, we see that the maximum reaction force generated is around 0.4N (Fig. 22). Although these forces are parasitic since the force sensor is mounted in the X direction and the motion is in the Z direction, a comparison can be made with the balanced case since the platform remains horizontal.

2) *Balanced:* In the balanced case, the masses are put back and the first experiment is conducted again. We see some peaks in the resulting plot (Fig. 23). These peaks are because the manufactured parts do not have a tight tolerance which leads to backlash therefore when the links are moved, they start and stop with a jerk. However, the forces are still low ($\approx 0.2N$)

In the second experiment, to imitate the starting conditions of the unbalanced situation, the platform is put to the lowest

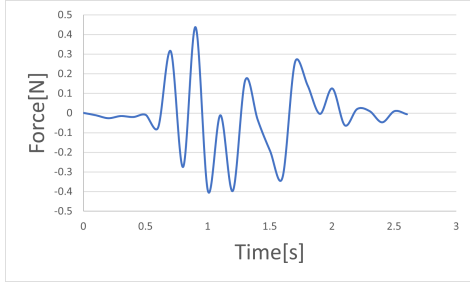


Fig. 22. Reaction force for unbalanced manipulator in the X direction for the experiment when the platform is moved up such that $\phi_{1i} = 40^\circ, i \in 1, 2, 3$, from its resting position (lowest potential)

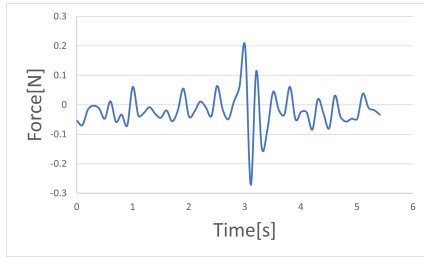


Fig. 23. Reaction forces in the case of an balanced manipulator in the X direction for the experiment when the platform is moved forward and back in the X direction. The motion is such $\phi_{11} = 40^\circ$ in the middle of the cycle.

position manually. From there, again the platform is raised such that $\phi_{1i} = 40^\circ$. We see that the maximum reaction force generated in the X direction is $\approx .2\text{N}$ (Fig.24).

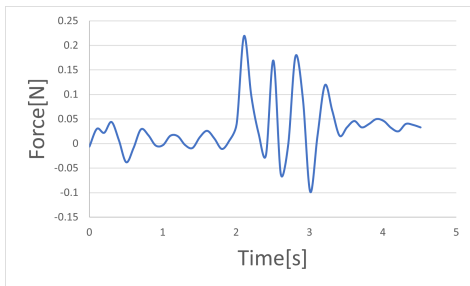


Fig. 24. Reaction force for balanced manipulator in the X direction for the experiment when the platform is moved up such that $\phi_{1i} = 40^\circ, i \in 1, 2, 3$, from the same position as the resting position of the unbalanced case

There is an offset in the steady state values in both cases after the trajectory is complete. It can be attributed to the way the force sensor is fixed to the base. There is a single thread screw screwed into the metal insert in the 3D printed base. This loose connection allows the metal screw to settle at a different inclined angle and thus not measure exact zero at the steady state in both the cases

It can be seen that the results obtained from experiments vary significantly from the simulations results. There are many factors that influenced the experiments that were not modeled in the simulations. Firstly, since the manufactured parts were hand-milled, they did not have a tight tolerance so there was al-

ways a backlash and extra jerk during at the beginning and the end of the motion cycle. Secondly, the since the components were not friction-less and the stiction in components were different, the component movement was different for an equal force. This again led to unexpected motion of the platform and consequently reaction forces. Thirdly, there were no damping in the simulations, this made a big difference especially in the unbalanced case where the platform falls down under its own weight due to gravity and then rises up unlike the damped situation in the real setup where the platform settles due to damping. No damping also affected the orientation angle of the platform making the simulation more different than the actual experiments. It can be realised that all these problems can be tackled using better manufactured parts and making the simulations include friction and damping.

IX. DISCUSSION

The manipulator was observed to be force-balanced not just for translations but even for cases when the platform does not remain parallel and has some orientation. This corroborates the platform mass equivalence model shown in Fig.5. Since the manipulator still has reaction moments, for complete dynamic balancing these moments have to be balanced. For a manipulator configuration like this, the angular momentum cannot be made constant passively using constraining methods [11]. If additional weight and power are not an issue then, active inertial wheels can be used such that sum of the angular momentum of the manipulator and the inertial wheels results in a constant value. [11]

Since ADAPT is forced balanced, it is not affected by gravity unlike statically-balanced mechanisms balanced with springs. ADAPT could be oriented in any direction, and it remains statically balanced. This would be useful, especially in surgical rooms where heavy instruments have to be handheld. The payload(instrument) could replace the platform such that its center of mass remains invariant and at the same position as the platform's center of mass. There is no need for active actuators, locks, or springs and the manipulator can be moved to any spot with the least effort from the surgeon. The surgeon theoretically would just have to work against friction and the manipulator would stay at the position where it is left.

Besides the operation modes described in the paper, two additional useful operation modes were identified that can be further looked into in the future. These operation modes are again forced-balanced as the manipulators still consist of forced-balanced pantograph legs. When the manipulator platform is in the plane of the base the constraints change. In the case when the ϕ_{3i} joint is fixed perpendicular to the base, the manipulator gets the same freedom space as the planar-3RRR manipulator.

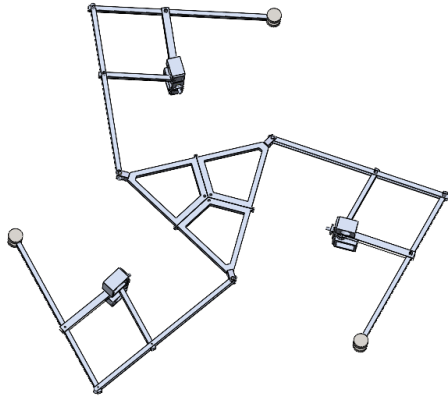


Fig. 25. The force balanced planar 3-RRR operation mode

Along the same lines, a force-balanced version of the 3RRR spherical parallel manipulator can be developed. Here the origin of the platform and the base coincide such that the constraint wrench consists of forces that span the full 3D space.



Fig. 26. The force balanced spherical parallel 3-RRR operation mode

This ability of the current manipulator to attain different operation modes can be achieved without the disassembly of the manipulator. Moreover, the manipulator stays in one operation mode unless it encounters a singularity point in its configuration space.

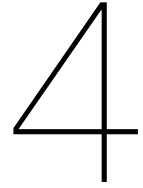
X. CONCLUSION

In this work, ADAPT, a force-balanced re-configurable spatial parallel manipulator with pantograph legs is introduced. The design is such that it shows different operation modes while being force balanced in its configuration space. The kinematics of the manipulator is formulated for the translation mode of operation and the forward and inverse kinematic Jacobians were derived. After identifying the singularities in the configuration space, the workspace was manually optimized using computer assistance. To validate the design for its force reactionless behavior, simulations were done for a simplified model on MSC ADAMS that showed the expected behavior. An experimental setup was also built to substantiate

the results of the simulation. The experiments showed that the manufactured parts have to be made with tighter tolerance to be completely reactionless however, the measured reaction forces were still substantially lower when the balanced case is compared to the unbalanced case (around 50 percent lesser). Two other force-balanced operation modes were also presented in the paper. One is a force-balanced version of the 3RRR planar robot and the other is a force-balanced version of a 3RRR rotary mechanism. These mechanisms have the potential to be employed for various industrial purposes. This can be part of future research work.

REFERENCES

- [1] Amazon Prime Air, 2016. [Online]. Available: <http://www.amazon.com/b?node=8037720011>
- [2] AEROARMS Project, 2014. [Online]. Available: <https://cordis.europa.eu/project/id/644271>
- [3] Ruggiero, Fabio, Vincenzo Lippiello, and Anibal Ollero. "Aerial manipulation: A literature review." *IEEE Robotics and Automation Letters* 3.3 (2018): 1957-1964.
- [4] Ollero, Anibal, et al. "Past, present, and future of aerial robotic manipulators." *IEEE Transactions on Robotics* 38.1 (2021): 626-645.
- [5] Bellicoso, Carmine Dario, et al. "Design, modeling and control of a 5-DoF light-weight robot arm for aerial manipulation." 2015 23rd Mediterranean Conference on Control and Automation (MED). IEEE, 2015.
- [6] Suarez, Alejandro, et al. "Design of a lightweight dual arm system for aerial manipulation." *Mechatronics* 50 (2018): 30-44.
- [7] Yang, Hyunsoo, and Dongjun Lee. "Dynamics and control of quadrotor with robotic manipulator." 2014 IEEE international conference on robotics and automation (ICRA). IEEE, 2014.
- [8] Yüksel, Burak, Gabriele Buondonno, and Antonio Franchi. "Differential flatness and control of protocentric aerial manipulators with any number of arms and mixed rigid/elastic-joints." 2016 IEEE/RSJ International Conference on Intelligent Robots and Systems (IROS). IEEE, 2016.
- [9] Mersha, Abeje Yenehun, Stefano Stramigioli, and Raffaella Carloni. "On bilateral teleoperation of aerial robots." *IEEE Transactions on Robotics* 30.1 (2013): 258-274.
- [10] Van der Wijk, V. "Methodology for analysis and synthesis of inherently force and momentbalanced mechanisms-theory and applications (dissertation)." University of Twente (free download: <http://dx.doi.org/10.3990/1.9789036536301>) (2014).
- [11] Wijk, V., and Justus Laurens Herder. "Dynamic balancing of Clavel's Delta robot." *Computational kinematics*. Springer, Berlin, Heidelberg, 2009. 315-322.
- [12] López, M., et al. "Delta robot: inverse, direct, and intermediate Jacobians." *Proceedings of the Institution of Mechanical Engineers, Part C: Journal of Mechanical Engineering Science* 220.1 (2006): 103-109.
- [13] Li, Yangmin, and Qingsong Xu. "Kinematic analysis and design of a new 3-DOF translational parallel manipulator." (2006): 729-737.
- [14] Tsai, Lung-Wen. *Robot analysis: the mechanics of serial and parallel manipulators*. John Wiley and Sons, 1999.
- [15] Zlatanov, Dimitar, Ilian A. Bonev, and Clément M. Gosselin. "Constraint singularities of parallel mechanisms." *Proceedings 2002 IEEE International Conference on Robotics and Automation (Cat. No. 02CH37292)*. Vol. 1. IEEE, 2002.
- [16] Mahmoodi, Mostafa, Mahmood Ghafouri Tabrizi, and Khalil Alipour. "A new approach for Kinematics-based design of 3-RRR delta robots with a specified workspace." 2015 AI and Robotics (IRANOPEN). IEEE, 2015.
- [17] Zlatanov, D., Bonev, I.A., and Gosselin, C.M., "Constraint Singularities as C-Space Singularities," 8th International Symposium on Advances in Robot Kinematics (ARK 2002), Caldes de Malavella, Spain, June 24-28, 2002.
- [18] Patel, Ketankumar H., et al. "Workspace and singularity analysis of 3-RRR planar parallel manipulator." *Proceedings of the 1st international and 16th national conference on machines and mechanisms*. 2013.



Discussion

4.1. Discussion

In chapter 2 various methods to design inherently dynamically balanced mechanisms were introduced and compared. It was found from the study that these mechanisms were lighter than the mechanisms where dynamic balancing is considered after kinematic synthesis. Four ways to dynamically balance mechanisms were discussed. Method of principle vectors, using dynamically balanced four bar elements as primary elements, reactionless path planning, and the leg-by-leg balancing approach. Inherent balancing always leads to a weight increase compared to the case where there is no balancing of reaction forces. This can be especially detrimental in cases where weight is a major constraint. Chapter 2 also showed that mechanisms built using the methods discussed were either low DoF mechanisms or the mechanisms became very heavy very quickly as the DoFs were increased. For higher DoF mechanisms mostly the leg-by-leg approach was used where each leg was force/dynamically balanced first and then combined to form a force/dynamically balanced higher DoF parallel structure. This way of creating a high DoF structure leads to bulkier systems.

It can also be seen that it is sometimes prudent to leave the mechanism partially balanced if the weight increases too much. For instance, on UAVs, control algorithms exist that make corrections to the trajectory in almost real-time without needing a mathematical model of the manipulator, treating the reaction forces as noise. If making the system fully balanced leads to a steep increase in complexity or weight, leaving the system just force-balanced would be a judicious choice.

It was seen that there are not many balanced mechanisms with prismatic joints. This is because symmetrical designs with prismatic joints are difficult to attain. Since the CoM has to be invariant in force balanced mechanism, it requires symmetry in design. Not having a balanced alternative to prismatic joints also hindered the development of higher DoF-balanced mechanisms that regularly use prismatic joints. It was also seen that just like how constraint wrenches can be directly added in parallel systems, the span of force/moment balance vectors could also be added.

These insights led to the development of ADAPT described in chapter 3. ADAPT involved the use of a pantograph as its legs. The pantographs (consisting of only revolute joints) were force balanced in their plane. Moreover, combining pantographs in parallel meant that balanced planes could be combined such that the combination spanned the full 3D space, making ADAPT a spatially force-balanced mechanism. This construction of ADAPT used fewer elements than the leg-by-leg balancing approach. The structure of the manipulator was found to be exactly similar to the DYMO robot, this meant that it shared the same motion operation modes. The configuration allowed for five different operation modes: translation, orientation, mixed (translation+orientation), planar, and lock-up. The focus of this work was on the development of a translation mechanism, therefore a kinematic model for only the translation mode was developed. If the active joint was put in the first position (controlling ϕ_{3i}) then there existed a singularity line where the platform would fall under its weight when the ϕ_{3i} were equal. To avoid this the second joint controlling ϕ_{1i} was made the active joint. This made the current manipulator different from the existing manipulators where the active joint is usually the first joint. Derivation of the Jacobian relating the input joint velocity to the output position velocities was also slightly different. Researchers have

usually employed generic analytical reductions to get rid of the passive variables from the Jacobian equations. However, these reductions did not work in the current manipulator and therefore geometrical relations were used for reduction. The Jacobian matrices were found to have the same structure as the ones for a Delta robot. However, it was not possible to find the null space of this kind of closed parallel structure analytically. These singularities were thus found by looking at similar architectures. The workspace volume of the manipulator was also manually optimized by considering the geometry of the manipulator and also the drone under which the manipulator was fixed. Since the optimization was done manually by changing the parameters individually and observing the effect on the workspace, an analytical model could be created in future research work to formulate a parametric optimization problem. Simulations were conducted on a simplified model in MSC ADAMS. The simulations showed that the manipulator was indeed reactionless for all motions in its workspace. The reaction forces were not exactly zero but in the order of 10^{-5} . This can be attributed to the numerical errors in simulation. To validate the simulations an experimental setup was built and experiments similar to the simulations were conducted. The experimental results showed that the reaction forces in the balanced case were lower than in the unbalanced case in all the situations. However, the experiments did not completely match the simulation results. The discrepancy was due to manufacturing defects in the hand-milled parts and non-ideal experimentation environment, unlike the simulations where there was no damping or friction. The problems can be solved by making the parts with tight tolerance and making the simulation environment more realistic.

4.2. Recommendations for Future Work

The results of this work show that it is possible to create a force-balanced manipulator that can be fixed underneath a drone. However, there are still many improvements and recommendations for future work that would help create a better model. .

1. **Development of a full kinematic model:** In the current work, the kinematic model for only translations has been developed as the manipulator was developed to be used for translation. It was seen that the manipulator could also show other motion modes. these included orientation, mixed, planar, and lockup. The advantage of this mechanism is that it stays as a 3-DoF mechanism unless a singularity point comes in its configuration space. This means that independent kinematic models could be developed for individual modes that could use implied constraints like in the current work to make the kinematic modeling simpler.
2. **Numerical Estimation of the workspace:** Since the Jacobian null space could not be found analytically. A cloud of equally spaced points could be created and tested point by point in the inverse kinematic model to see if it lies within the workspace. This was tried in the current research work as well but the algorithm was taking too much time to solve. A better algorithm could be developed to do the same.
3. **Analytical model for workspace optimization:** In the current work, a crude manual way was used to map the platform workspace when it intersected the drone. Although this method gave an idea of workspace, the workspace could not be optimized since there was no parametric relation. The geometry of the drone and the manipulator can be mathematically formulated so that intersections can be identified. A parametric mathematical definition can be converted into an optimization problem. This would give better results than manual optimization in this work. An analytical model is provided in Appendix C that can be further improved by including the drone body.
4. **Realistic simulation environment on MSC ADAMS:** Although the simulation results were as expected. A more realistic environment could be created with friction and damping so that there is very less discrepancy between the simulation environment and the actual setup.
5. **Better products and manufactured parts:** In the current manipulator, the components were hand-milled and so the manufacturing errors were more. In the future, the parts could be manufactured on CNC machines such that they have tighter tolerance. This would also reduce the backlash in the system which leads to unwanted reaction forces. The links were connected to

each other using readily available screw threads that led to additional friction for the relative motion between the links. Shoulder bolts or something similar could be used in the next iteration to solve this problem.

6. **Exploring other architectures of the robot:** Since the robot is reconfigurable without disassembly, it could show different operation modes. Only translation mode was explored in this work. Two other useful configurations that could be used in the industry are the force-balanced 3-RRR planar translation mechanism and the force-balanced 3-RRR orientation mechanism. The planar translation 3-RRR mechanism can be formed by fixing the ϕ_{3i} angle perpendicular to the plane. Similarly when the ϕ_{3i} angle is not fixed but the origin of the platform and the base coincide then the manipulator becomes a 3-DoF orientation mechanism. The constraint wrench consists of forces whose combination in this case spans the full 3D space.

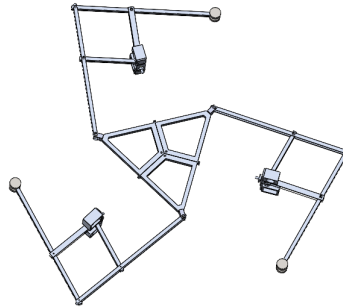


Figure 4.1: The force balanced planar 3-RRR operation mode



Figure 4.2: The force-balanced spherical parallel 3-RRR operation mode

7. **Moment balancing:** The moment can be balanced by making the angular momentum constant in a mechanism. In ADAPT there is angular momentum in all three axes. To make the angular momentum constant, actively driven inertia wheels can be added such that the sum of angular momentum from the active inertial disks and the ADAPT manipulator is constant. A single unit as proposed in [27] can be put in a compact box and fixed to the manipulator.

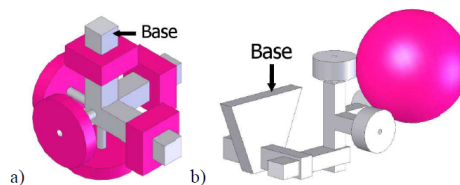


Figure 4.3: Schematic model of active balancing units. Motors have not been included but can be fixed to counterweights. a) One balancing element for each DoF b) One balancing element for all DoFs [27]

5

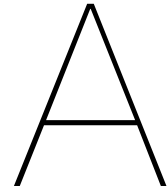
Conclusion

In this work methods of inherent balancing were first explored and compared. These mechanisms are constructed such that each element serves the dual purpose of motion and dynamic balancing. The inherent balancing methods were divided into four categories: Mechanisms based on the method of principal vectors, the method of balanced four bars, the method of reactionless path planning, and the leg-by-leg approach. It was concluded in their comparison that each method had its advantages and disadvantages. A table was presented at the end of Chapter 2 that graded the methods on various parameters. The work also presented the design, development and validation of the ADAPT manipulator in Chapter 3. The construction of ADAPT consisting of pantograph legs was such that it was spatially forced balanced. ADAPT could also be reconfigured to show different motion operation modes without disassembly. Modes included spatial translation, orientation, mixed mode(translation+orientation), planar and lockup. In this work, only spatial transnational mode was studied. A kinematic model was developed for this spatial translation mode of operation. Singularities were identified for ADAPT and workspace volume was found geometrically. To test the force-balance nature, simulations were conducted on the simplified models of the ADAPT in MSC ADAMS multibody simulation software. The results of the simulation confirmed that the ADAPT manipulator is reactionless for all the motions in its configuration space. An experimental setup was also built to validate the simulation results. The experiments although not ideal showed that the reaction forces in the balanced case were always significantly smaller (half or less) than in the unbalanced case. Apart from ADAPT, two additional force-balanced configurations were proposed. One is the force-balanced planar 3-RRR mechanism and the other is the force-balanced orientation mechanism. Studying these designs could be part of future work.

Bibliography

- [1] Wikipedia contributors, *Butterfly effect* — *Wikipedia, the free encyclopedia*, [Online; accessed 27-August-2022], 2022. [Online]. Available: https://en.wikipedia.org/w/index.php?title=Butterfly_effect&oldid=1105034134.
- [2] *Balance of nature* — *Wikipedia, the free encyclopedia*, [Online; accessed 24-August-2022], 2022. [Online]. Available: https://en.wikipedia.org/w/index.php?title=Balance_of_nature&oldid=1099103830.
- [3] *Entropy* — *Wikipedia, the free encyclopedia*, [Online; accessed 24-August-2022], 2022. [Online]. Available: <https://en.wikipedia.org/w/index.php?title=Entropy&oldid=1106307463>.
- [4] G. Lowen and R. Berkof, "Survey of investigations into the balancing of linkages," *Journal of mechanisms*, vol. 3, no. 4, pp. 221–231, 1968.
- [5] B. Wei and D. Zhang, "A review of dynamic balancing for robotic mechanisms," *Robotica*, vol. 39, no. 1, pp. 55–71, 2021.
- [6] H. Yang and D. Lee, "Dynamics and control of quadrotor with robotic manipulator," in *2014 IEEE international conference on robotics and automation (ICRA)*, IEEE, 2014, pp. 5544–5549.
- [7] B. Yüksel, G. Buondonno, and A. Franchi, "Differential flatness and control of protocentric aerial manipulators with any number of arms and mixed rigid-/elastic-joints," in *2016 IEEE/RSJ International Conference on Intelligent Robots and Systems (IROS)*, IEEE, 2016, pp. 561–566.
- [8] A. Y. Mersha, S. Stramigioli, and R. Carloni, "On bilateral teleoperation of aerial robots," *IEEE Transactions on Robotics*, vol. 30, no. 1, pp. 258–274, 2013.
- [9] A. D. Nashif, D. I. Jones, and J. P. Henderson, *Vibration damping*. John Wiley & Sons, 1991.
- [10] A. Suarez, A. E. Jimenez-Cano, V. M. Vega, G. Heredia, A. Rodriguez-Castaño, and A. Ollero, "Design of a lightweight dual arm system for aerial manipulation," *Mechatronics*, vol. 50, pp. 30–44, 2018.
- [11] V. van der Wijk, J. L. Herder, and B. Demeulenaere, "Comparison of various dynamic balancing principles regarding additional mass and additional inertia," 2009.
- [12] V. Van der Wijk, "Methodology for analysis and synthesis of inherently force and momentbalanced mechanisms-theory and applications (dissertation)," *University of Twente (free download: <http://dx.doi.org/10.3990/1.9789036536301>)*, 2014.
- [13] C. M. Gosselin, F. Vollmer, G. Côté, and Y. Wu, "Synthesis and design of reactionless three-degree-of-freedom parallel mechanisms," *IEEE Transactions on Robotics and Automation*, vol. 20, no. 2, pp. 191–199, 2004.
- [14] Y. Wu and C. M. Gosselin, "Synthesis of reactionless spatial 3-dof and 6-dof mechanisms without separate counter-rotations," *The International Journal of Robotics Research*, vol. 23, no. 6, pp. 625–642, 2004.
- [15] Y. Wu and C. Gosselin, "Design of reactionless 3-dof and 6-dof parallel manipulators using parallelepiped mechanisms," *IEEE Transactions on Robotics*, vol. 21, no. 5, pp. 821–833, 2005.
- [16] Y. Wu and C. M. Gosselin, "On the dynamic balancing of multi-dof parallel mechanisms with multiple legs," 2007.
- [17] Y. Wu, "Synthesis and analysis of reactionless spatial parallel mechanisms," Ph.D. dissertation, Ph. D. Dissertation (Laval University, 2003), 2003.
- [18] V. Wijk and J. L. Herder, "Dynamic balancing of clavel's delta robot," in *Computational kinematics*, Springer, 2009, pp. 315–322.

- [19] S. Foucault and C. m. M. Gosselin, "On the development of a planar 3-dof reactionless parallel mechanism," in *International Design Engineering Technical Conferences and Computers and Information in Engineering Conference*, American Society of Mechanical Engineers, vol. 36533, 2002, pp. 985–993.
- [20] S. K. Agrawal and A. Fattah, "Reactionless space and ground robots: Novel designs and concept studies," *Mechanism and Machine theory*, vol. 39, no. 1, pp. 25–40, 2004.
- [21] —, "Gravity-balancing of spatial robotic manipulators," *Mechanism and machine theory*, vol. 39, no. 12, pp. 1331–1344, 2004.
- [22] A. Fattah and S. K. Agrawal, "On the design of reactionless 3-dof planar parallel mechanisms," *Mechanism and Machine theory*, vol. 41, no. 1, pp. 70–82, 2006.
- [23] V. Van der Wijk and J. L. Herder, "Synthesis method for linkages with center of mass at invariant link point—pantograph based mechanisms," *Mechanism and machine theory*, vol. 48, pp. 15–28, 2012.
- [24] S. Briot, V. Arakelian, and S. Guégan, "Paminsa: A new family of partially decoupled parallel manipulators," *Mechanism and Machine Theory*, vol. 44, no. 2, pp. 425–444, 2009.
- [25] S. Briot and I. A. Bonev, "Pantopteron: A new fully decoupled 3dof translational parallel robot for pick-and-place applications," 2009.
- [26] —, "Pantopteron-4: A new 3t1r decoupled parallel manipulator for pick-and-place applications," *Mechanism and Machine Theory*, vol. 45, no. 5, pp. 707–721, 2010.
- [27] V. van der Wijk and J. L. Herder, "Active dynamic balancing unit for controlled shaking force and shaking moment balancing," in *International Design Engineering Technical Conferences and Computers and Information in Engineering Conference*, vol. 44106, 2010, pp. 1515–1522.
- [28] D. Zlatanov, R. G. Fenton, and B. Benhabib, "Singularity analysis of mechanisms and robots via a motion-space model of the instantaneous kinematics," in *Proceedings of the 1994 IEEE International Conference on Robotics and Automation*, IEEE, 1994, pp. 980–985.
- [29] R. D. Gregorio and V. Parenti-Castelli, "A translational 3-dof parallel manipulator," in *Advances in robot kinematics: analysis and control*, Springer, 1998, pp. 49–58.



Design Considerations

In this appendix the mass and length of various components is listed. How the masses and lengths were selected is further elaborated. This would allow the reader to follow the same thought process for replicating the design.

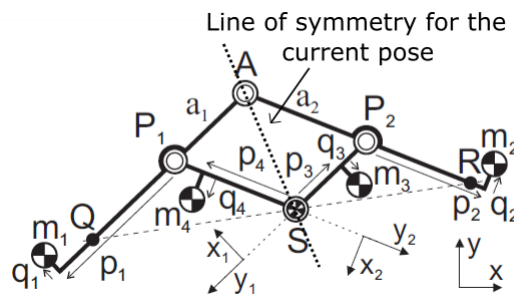


Figure A.1: General 2-DoF pantograph structure with the centre of mass of the structure at point S. The pantograph is mass symmetric about the instantaneous line joining points A and S. Since the legs are mass symmetric therefore the q 's have a value of zero.

To make the calculations easier the pantograph was made symmetric. To make it symmetric, masses m_1 were made equal to m_2 , m_3 equal to m_4 . Similarly, lengths p_3 was made equal to p_4 , a_1 equal to a_2 and p_1 equal to p_2 (Fig.A.1). This meant that just two equations needed to be solved in the forced balanced conditions(Chapter 3, Eq.4) . Once the mass and length of the short link was determined as elaborated in (Chapter 3, Section VII), the masses and the lengths of the other links could be determined. A length of 170mm was chosen since it was closest to the optimized values for the short link. For two short plates the mass was found to be 26g. Having made these selections and fixing the length of the longer arm such that p_1 was 160mm (with 167g allotted), a total mass of the three pantographs was calculated to be of 1.818Kgs. This was within the 2Kg limit set on the total mass of the manipulator and hence it provided some elbow room for masses of motors and base platform to be added later. After the addition of other motors and the base platform the full assembly weighed 1.975Kgs. A simple Matlab script was developed to do these calculations. The mass of the motor assembly (bottom most exploded view in Fig. A.2) does not need to be accounted in the moving pantograph assembly since the center of mass of the motor assembly is located at the invariant point S (Fig. A.1). However, the center of mass should be in the middle since an imbalance can still effect the ϕ_{3i} angular joint. However, the mass had to be included in the total mass so was kept as low as possible. The universal bottom assembly has been added to the platform mass as there is no relative motion between the platform and the joint. The mass of the base platform does not matter as it is fixed. Similarly, the components attached rigidly to the base platform(shown with a cross in the picture) have not been accounted in the moving pantograph.

Table A.1: Length of various components in the manipulator. The theoretically calculated values of lengths in the pantograph are listed at the end for reference

Component Name	Length(in mm)
Long square and Long plates	375
Short Square and short plates	150
Pantograph Elements	Length(in mm)
a1=a2	150
p3=p4	75
p1=p2	161.9

Table A.2: The theoretically calculated values of masses in the pantograph.

Pantograph element	Mass(in gms)
m1=m2	167
m3=m4	26

Table A.3: Masses of various components in the manipulator.

Mass of various components(in grams)	Leg-1	Leg-2	Leg-3
Long square	32.775	32.728	32.862
Shaft universal	1.629	1.597	5415
Universal bottom	11.494	11.587	11.599
Long plate 1	30.79	31.137	30.851
Long plate 2	31.112	30.067	30.988
Motor Counter-mass	56.39	56.278	56.264
Short Square	13.79	14.223	13.810
Short plate 1	12.945	13.065	13.039
M2 setscrew 4mm	.045	.045	.045
short plate 2	13.065	13.035	13.039
M2 setscrew 8mm	.12	.12	.12
Motor Joint	2.28	2.071	2.157
Motor spacer	.1	.1	.1
M2.5 motor setscrew	.436	.436	.436
M2.5 Motor counter mass setscrew	.385	.385	.385
Base Universal	25.45	25.37	25.293
M4 setscrew	2.140	2.140	2.140
Motor	56.4	56.4	56.4
Platform mass	206.6/3	206.6/3	206.6/3

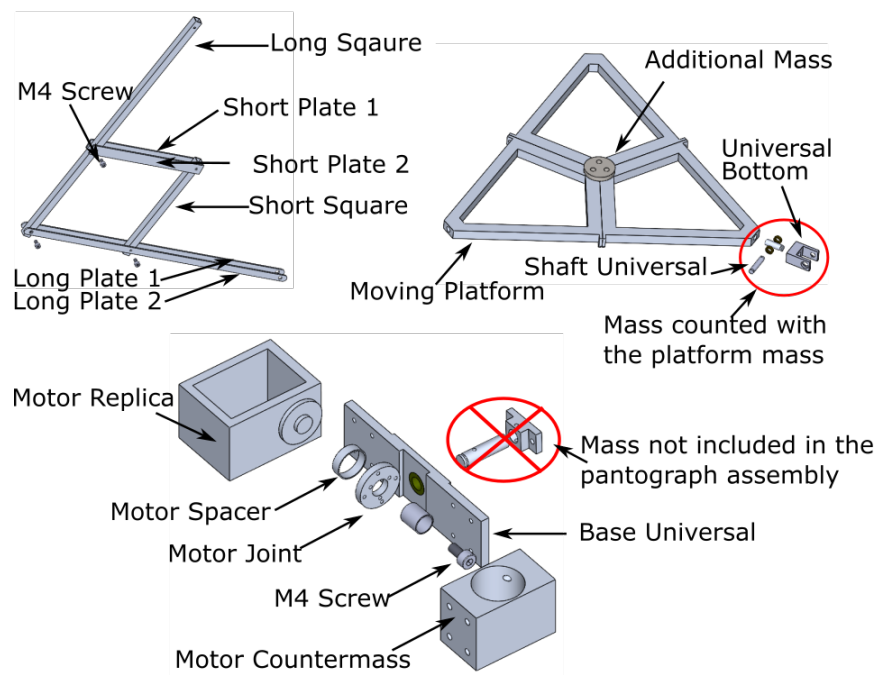


Figure A.2: Nomenclature of the various components used in the table.

B

Kinematics (Elaborated)

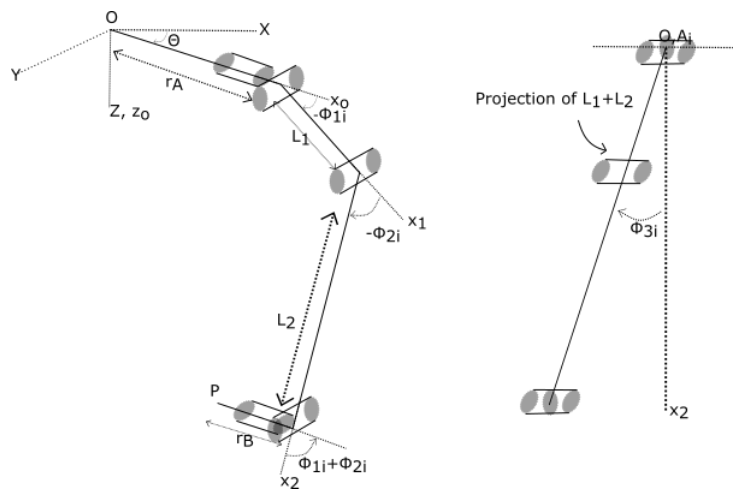


Figure B.1: Schematic diagram of one of the legs with the kinematic parameters.

In this appendix the kinematics shared in Section 3 of Chapter 3 is further expanded. Since almost all the transformation matrices for all the legs are similar, The matrices of only one of the leg is elaborated here. This leg is oriented such that θ_i angle is zero. To locate the position of point P of the moving platform Denavit-Hartenberg transformation matrices are defined. The transformation matrices are 4x4 homogeneous matrices with a 3x3 rotation component on the left and a 3x1 position vector on the right of the matrix. Generic three rotation matrices and three translation matrices are shown below.

$$R_{x(\alpha)} = \begin{bmatrix} 1 & 0 & 0 & 0 \\ 0 & C_\alpha & -S_\alpha & 0 \\ 0 & S_\alpha & C_\alpha & 0 \\ 0 & 0 & 0 & 1 \end{bmatrix} \quad R_{y(\alpha)} = \begin{bmatrix} C_\alpha & 0 & S_\alpha & 0 \\ 0 & 1 & 0 & 0 \\ -S_\alpha & 0 & C_\alpha & 0 \\ 0 & 0 & 0 & 1 \end{bmatrix} \quad R_{z(\alpha)} = \begin{bmatrix} C_\alpha & -S_\alpha & 0 & 0 \\ S_\alpha & C_\alpha & 0 & 0 \\ 0 & 0 & 1 & 0 \\ 0 & 0 & 0 & 1 \end{bmatrix} \quad (B.1)$$

$$T_{x(d)} = \begin{bmatrix} 1 & 0 & 0 & d \\ 0 & 1 & 0 & 0 \\ 0 & 0 & 1 & 0 \\ 0 & 0 & 0 & 1 \end{bmatrix} \quad T_{y(d)} = \begin{bmatrix} 1 & 0 & 0 & 0 \\ 0 & 1 & 0 & d \\ 0 & 0 & 1 & 0 \\ 0 & 0 & 0 & 1 \end{bmatrix} \quad T_{z(d)} = \begin{bmatrix} 1 & 0 & 0 & 0 \\ 0 & 1 & 0 & 0 \\ 0 & 0 & 1 & d \\ 0 & 0 & 0 & 1 \end{bmatrix} \quad (B.2)$$

Where S() and C() are used for sin and cos functions respectively for brevity. Benefit of homogeneous matrices is that they can be directly multiplied to get the transformation from one frame to the next. For instance, transformation matrix T_{r_z} when multiplied to T_{r_α} makes the coordinate transformation from the reference frame at the base (XYZ) to the reference frame at the leg attachment point. The intermediate frames have not be represented in the figure for the sake of clarity. The transformation matrices have been defined so that the x axis is always along the link. Individual matrices have been defined below that makes the coordinate transformation from its local origin to the origin of the next frame of reference.

$$\begin{aligned}
T_{rz} &= \begin{pmatrix} \cos(\theta_i) & -\sin(\theta_i) & 0 & 0 \\ \sin(\theta_i) & \cos(\theta_i) & 0 & 0 \\ 0 & 0 & 1 & 0 \\ 0 & 0 & 0 & 1 \end{pmatrix} & T_{tra} &= \begin{pmatrix} 1 & 0 & 0 & ra \\ 0 & 1 & 0 & 0 \\ 0 & 0 & 1 & 0 \\ 0 & 0 & 0 & 1 \end{pmatrix} \\
T_{rxo} &= \begin{pmatrix} 1 & 0 & 0 & 0 \\ 0 & \cos(\phi_{31}) & \sin(\phi_{31}) & 0 \\ 0 & -\sin(\phi_{31}) & \cos(\phi_{31}) & 0 \\ 0 & 0 & 0 & 1 \end{pmatrix} & T_{ryo} &= \begin{pmatrix} \cos(\phi_{11}) & 0 & -\sin(\phi_{11}) & 0 \\ 0 & 1 & 0 & 0 \\ \sin(\phi_{11}) & 0 & \cos(\phi_{11}) & 0 \\ 0 & 0 & 0 & 1 \end{pmatrix} \\
T_{tL1} &= \begin{pmatrix} 1 & 0 & 0 & L_1 \\ 0 & 1 & 0 & 0 \\ 0 & 0 & 1 & 0 \\ 0 & 0 & 0 & 1 \end{pmatrix} & T_{ry1} &= \begin{pmatrix} \cos(\phi_{21}) & 0 & -\sin(\phi_{21}) & 0 \\ 0 & 1 & 0 & 0 \\ \sin(\phi_{21}) & 0 & \cos(\phi_{21}) & 0 \\ 0 & 0 & 0 & 1 \end{pmatrix} \\
T_{tL2} &= \begin{pmatrix} 1 & 0 & 0 & L_2 \\ 0 & 1 & 0 & 0 \\ 0 & 0 & 1 & 0 \\ 0 & 0 & 0 & 1 \end{pmatrix} & T_{ry2} &= \begin{pmatrix} \cos(\phi_{11} + \phi_{21}) & 0 & \sin(\phi_{11} + \phi_{21}) & 0 \\ 0 & 1 & 0 & 0 \\ -\sin(\phi_{11} + \phi_{21}) & 0 & \cos(\phi_{11} + \phi_{21}) & 0 \\ 0 & 0 & 0 & 1 \end{pmatrix} \\
T_{rxz} &= \begin{pmatrix} 1 & 0 & 0 & 0 \\ 0 & \cos(\phi_{31}) & -\sin(\phi_{31}) & 0 \\ 0 & \sin(\phi_{31}) & \cos(\phi_{31}) & 0 \\ 0 & 0 & 0 & 1 \end{pmatrix} & T_{trb} &= \begin{pmatrix} 1 & 0 & 0 & -rb \\ 0 & 1 & 0 & 0 \\ 0 & 0 & 1 & 0 \\ 0 & 0 & 0 & 1 \end{pmatrix} \\
T_{rzz} &= \begin{pmatrix} \cos(\theta_i) & \sin(\theta_i) & 0 & 0 \\ -\sin(\theta_i) & \cos(\theta_i) & 0 & 0 \\ 0 & 0 & 1 & 0 \\ 0 & 0 & 0 & 1 \end{pmatrix}
\end{aligned} \tag{B.3}$$

The sequence of matrix multiplication results in the transformation from the base frame to the platform frame. The resultant transformation matrix from the fixed frame to the frame attached to the platform center can be written as

$$T_r p = T_{rz} T_{tra} T_{rxo} T_{ryo} T_{tL1} T_{ry1} T_{tL2} T_{ry2} T_{rxz} T_{trb} T_{rzz} = \begin{bmatrix} R_{3 \times 3} & P_{3 \times 1} \\ 0_{1 \times 3} & 1 \end{bmatrix} \tag{B.4}$$

where R is an identity matrix since the platform does not have any rotations, P can be written as

$$\begin{pmatrix} ra C(\theta_i) - rb C(\theta_i) + L_1 C(\phi_{11}) C(\theta_i) + L_2 C(\phi_{11}) C(\phi_{21}) C(\theta_i) - L_2 C(\theta_i) S(\phi_{11}) S(\phi_{21}) - L_1 S(\phi_{11}) S(\phi_{31}) S(\theta_i) - L_2 C(\phi_{11}) S(\phi_{21}) S(\phi_{31}) S(\theta_i) - L_2 C(\phi_{21}) S(\phi_{11}) S(\phi_{31}) S(\theta_i) \\ ra S(\theta_i) - rb S(\theta_i) + L_1 C(\phi_{11}) S(\theta_i) + L_2 C(\phi_{11}) C(\phi_{21}) S(\theta_i) + L_1 C(\theta_i) S(\phi_{11}) S(\phi_{31}) - L_2 S(\phi_{11}) S(\phi_{21}) S(\theta_i) + L_2 C(\phi_{11}) C(\theta_i) S(\phi_{21}) S(\phi_{31}) + L_2 C(\phi_{21}) C(\theta_i) S(\phi_{11}) S(\phi_{31}) \\ C(\phi_{31}) (L_2 S(\phi_{11} + \phi_{21}) + L_1 S(\phi_{11})) \end{pmatrix} \tag{B.5}$$

Where $S()$ and $C()$ are used for sin and cos functions respectively for brevity. As explained in the inverse kinematics section, the goal is to find the angular location of the active joint for some specific value of the position of the moving platform. It can be seen in the figure that the magnitude of the vector joining O and P does not depend on the passive variable ϕ_{31} since the leg is planar, only the planar components matter in its magnitude. We can see this by assuming all the joints to be constant and varying ϕ_{31} variable, the magnitude of the vector OP remains the same even when ϕ_{31} changes. Therefore the leg forms a circle with radius C as can be seen in the figure in yellow. We can calculate the length of the vector by squaring and adding the x,y,z position equations in the transformation matrix.

$$\begin{aligned}
T_{rp}(1,4)^2 + T_{rp}(2,4)^2 + T_{rp}(3,4)^2 &= px^2 + py^2 + pz^2 \\
&= L_1^2 + 2 \cos(\phi_{21}) L_1 L_2 + 2 \cos(\phi_{11}) L_1 ra + L_2^2 + 2 \cos(\phi_{11} + \phi_{21}) L_2 ra + ra^2 + rb^2 = px^2 + \\
&py^2 + pz^2 + 2 ra rb + 2 L_2 rb \cos(\phi_{11} + \phi_{21}) + 2 L_1 rb \cos(\phi_{11})
\end{aligned} \tag{B.6}$$

Doing that we see that the dependence on ϕ_{3i} indeed falls off and we can get a relation between ϕ_{21} and ϕ_{11} . We can substitute ϕ_{21} in the z position equation in the transformation matrix and find a

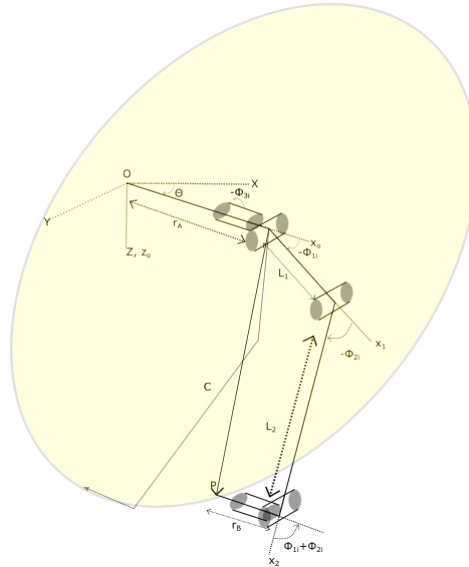


Figure B.2: Schematic diagram of one of the legs with the kinematic parameters. When all the joints are kept fixed and only ϕ_{3i} is allowed to move then the leg end point forms a circle with a fixed radius. This radius (C) is independent of the joint variable ϕ_{3i}

relation between ϕ_{11} and ϕ_{31} . The equation is still very long to present here so it has been omitted. Substituting the value of ϕ_{2i} in the z position equation and we get a relation between ϕ_{3i} and ϕ_{1i} . We can then substitute the known values of ϕ_{3i} , and ϕ_{2i} in terms of ϕ_{11} in x position equation to find the value of ϕ_{1i} in terms of the known position variables p_x , p_y and p_z . The following equation relates ϕ_{1i} and p_x , p_y and p_z .

$$p_x + r_b \cos(\theta) + L_1 \sin(\phi_{11}) \sin(\theta) \sigma_1 + L_2 \cos(\theta) \sin(\phi_{11}) \sin(\sigma_2) + L_2 \cos(\phi_{11}) \sin(\theta) \sin(\sigma_2) \sigma_1 + L_2 \cos(\sigma_2) \sin(\phi_{11}) \sin(\theta) \sigma_1 = \cos(\theta) (r_a + L_1 \cos(\phi_{11}) + L_2 \cos(\phi_{11}) \cos(\sigma_2)) \quad (\text{B.7})$$

where σ_1 and σ_2 are functions of ϕ_{1i} and p_x , p_y and p_z that have been omitted here for the sake of brevity.

Since ϕ_{11} is the active joint once the equation in terms of ϕ_{11} is derived, the jacobian can be evaluated to find the platform velocity with respect to the derivative of the input joint variables $\dot{\phi}_{1i}$ is for all the legs. The equation can be represented in the following form

$$J_p * v = J_\theta * \dot{\theta} \quad (\text{B.8})$$

where J_θ is,

$$J_\theta = \begin{pmatrix} A & 0 & 0 \\ 0 & B & 0 \\ 0 & 0 & C \end{pmatrix}$$

where

$$A = L_1 \sin(\phi_{11}) + L_2 \cos(\phi_{11}) \sin(\sigma_9) + L_2 \cos(\sigma_9) \sin(\phi_{11}) + \frac{2 L_2 \cos(\phi_{11}) \sin(\sigma_9) \sigma_3}{\sigma_4} + \frac{2 L_2 \cos(\sigma_9) \sin(\phi_{11}) \sigma_3}{\sigma_4},$$

$$B = L_1 \sin(\phi_{12}) + L_2 \cos(\phi_{12}) \sin(\sigma_8) + L_2 \cos(\sigma_8) \sin(\phi_{12}) + \frac{2 L_2 \cos(\phi_{12}) \sin(\sigma_8) \sigma_2}{\sigma_5} + \frac{2 L_2 \cos(\sigma_8) \sin(\phi_{12}) \sigma_2}{\sigma_5}$$

$$C = L_1 \sin(\phi_{13}) + L_2 \cos(\phi_{13}) \sin(\sigma_7) + L_2 \cos(\sigma_7) \sin(\phi_{13}) + \frac{2 L_2 \cos(\phi_{13}) \sin(\sigma_7) \sigma_1}{\sigma_6} + \frac{2 L_2 \cos(\sigma_7) \sin(\phi_{13}) \sigma_1}{\sigma_6}$$

(B.9)

Here, again the values of σ 's have been omitted for the sake of brevity (The exact values do not matter as the null space cannot be found. However, the jacobian structure helps in identifying the behaviour of the manipulator). Where J_θ is a diagonal matrix which implies that the input velocities are independent of each other when moving the platform, which is similar to a conventional Delta robot.

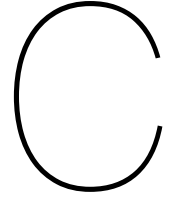
$$J_p = \begin{pmatrix} D \\ E \\ F \end{pmatrix}$$

where,

$$\begin{aligned} D &= \text{pxd} \left(\frac{2 L_2 \cos(\sigma_{13}) \sin(\phi_{11}) \sigma_{12}}{\sigma_3} - 1 \right) + \frac{2 L_2 \text{pxd} \cos(\phi_{11}) \sin(\sigma_{13}) \sigma_{12}}{\sigma_3} + \\ &\frac{2 L_2 \text{pyd} \cos(\phi_{11}) \sin(\sigma_{13}) \sigma_9}{\sigma_3} + \frac{2 L_2 \text{pyd} \cos(\sigma_{13}) \sin(\phi_{11}) \sigma_9}{\sigma_3} + \\ &\frac{2 L_2 \text{pzd} \cos(\phi_{11}) \sin(\sigma_{13}) \sigma_6}{\sigma_3} + \frac{2 L_2 \text{pzd} \cos(\sigma_{13}) \sin(\phi_{11}) \sigma_6}{\sigma_3} \\ E &= \text{pxd} \left(\frac{2 L_2 \cos(\sigma_{14}) \sin(\phi_{12}) \sigma_{11}}{\sigma_2} - 1 \right) + \frac{2 L_2 \text{pxd} \cos(\phi_{12}) \sin(\sigma_{14}) \sigma_{11}}{\sigma_2} + \\ &\frac{2 L_2 \text{pyd} \cos(\phi_{12}) \sin(\sigma_{14}) \sigma_8}{\sigma_2} + \frac{2 L_2 \text{pyd} \cos(\sigma_{14}) \sin(\phi_{12}) \sigma_8}{\sigma_2} + \\ &\frac{2 L_2 \text{pzd} \cos(\phi_{12}) \sin(\sigma_{14}) \sigma_5 \sigma_2}{\sigma_2} + \frac{2 L_2 \text{pzd} \cos(\sigma_{14}) \sin(\phi_{12}) \sigma_5}{\sigma_2} \\ F &= \text{pxd} \left(\frac{2 L_2 \cos(\sigma_{15}) \sin(\phi_{13}) \sigma_{10}}{\sigma_1} - 1 \right) + \frac{2 L_2 \text{pxd} \cos(\phi_{13}) \sin(\sigma_{15}) \sigma_{10}}{\sigma_1} + \\ &\frac{2 L_2 \text{pyd} \cos(\phi_{13}) \sin(\sigma_{15}) \sigma_7}{\sigma_1} + \frac{2 L_2 \text{pyd} \cos(\sigma_{15}) \sin(\phi_{13}) \sigma_7}{\sigma_1} + \\ &\frac{2 L_2 \text{pzd} \cos(\phi_{13}) \sin(\sigma_{15}) \sigma_4}{\sigma_1} + \frac{2 L_2 \text{pzd} \cos(\sigma_{15}) \sin(\phi_{13}) \sigma_4}{\sigma_1} \end{aligned} \quad (\text{B.10})$$

Once again the values of σ 's have been omitted for the sake of brevity. J_p is a full matrix indicating

that the velocity in all the three axis is effected by a single input, again similar to a conventional Delta robot. It can be noticed from the Jacobian matrices that an exact solution for null space to calculate the singularity is almost impossible to get, so the singularities cannot be found analytically. This corroborates with most closed loop parallel manipulators where only input and output equations are used in the development of the kinematic model [28]. To develop a model which does not miss singularities full velocity equation needs to be developed where the passive joint velocities are also accounted [29]. This can be looked into in the future.



Workspace

C.1. Analytical Workspace Estimation without the drone body

The Maximum Surrounded Workspace (MSW) resulting in a solid volume can be formulated analytically by identifying the reach limits of a single leg of the manipulator. The reach limits defines the available planar surface for a single leg which can then be revolved to get the solid volume. The surface is the area enclosed between a circle and two lines. The lines and circles are defined as follows

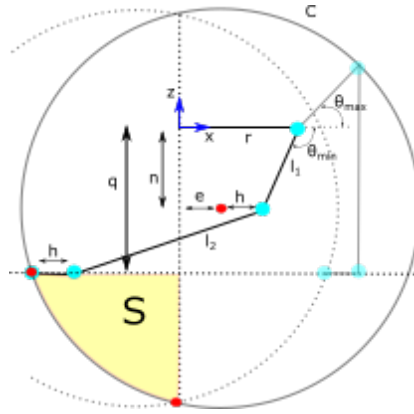


Figure C.1: Planar reach limits of one of the legs. The workspace solid volume can be found by revolving the surface S around the central axis.

$$\begin{aligned}
 L_1 &: x = 0 \\
 L_2 &: z = -q \\
 C &: (x - e)^2 + (z + n)^2 = l_2^2 \\
 \text{Where,} \\
 Q &= l_2 - l_1 \sin \theta_{max} \\
 e &= r - h + l_1 \cos \theta_{min} \\
 n &= l_1 \sin \theta_{min}
 \end{aligned}$$

where θ_{min} and θ_{max} are the rotational limits on the active joints. The area enclosed can be calculated by

$$\begin{aligned}
 \text{Area} &= (l_2^2/2) * (\pi/2 - \arcsin(x/l_2) - \arcsin(z/l_2)) \\
 &- (1/2) * (x * \sqrt{(l_2^2 - x^2)} + (z) * \sqrt{(l_2^2 - (z)^2)} - 2 * x * z)
 \end{aligned} \tag{C.1}$$

With this method the workspace volume generated is greater than what would be in the actual case as there are theoretically no limits on the values of θ_{min} and θ_{max} without the drone body. However, this method is still useful to get preliminary values for further optimization.

C.2. Computer Assisted Manual Optimization

As mentioned in the section Chapter 3, Section 5, Maximum Surrounded Workspace helps in visualizing the workspace facilitating a kinematic based design. The leg parameters R, L_1, L_2 and r were identified as the parameters affecting the reach limits of the leg. These reach limits helped generate a surface, which when revolved, developed the workspace volume. Since an analytical model with all these parameters affecting the workspace simultaneously could not be formulated, each parameter was varied individually and their effect on the workspace volume was noted. The starting values of the parameters were as follows; $R = 250mm, L_1 = 150mm, L_2 = 170mm$ and $r = 200mm$.

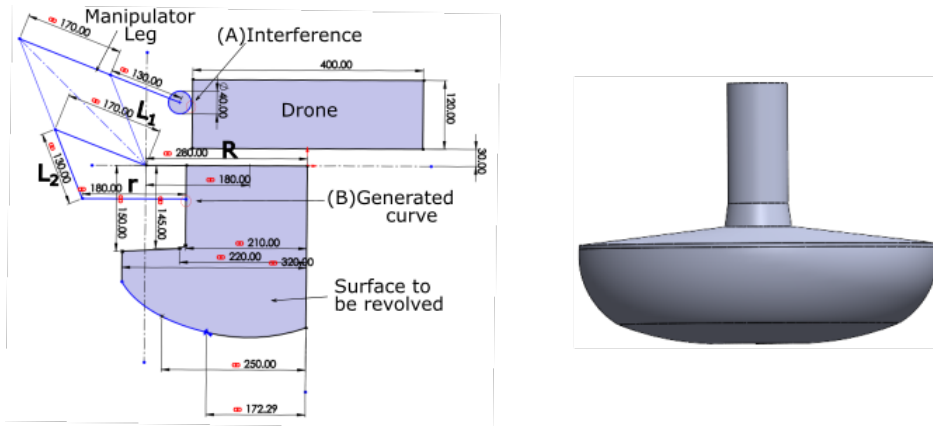


Figure C.2: Left: Planar reach limits of one of the legs. The workspace solid volume can be found by revolving the surface S around the central axis. Right: The workspace shape and volume with the starting values.

With increasing r it was seen that the workspace volume decreases. It can be attributed to the fact that as r is increased, the centre point of the platform comes closer to the axis of rotation thus reducing the volume. When L_1 is increased it leads to increase in the workspace volume, this is straightforward to see since increase in L_1 leads to an increase in turning radius the pantograph which directly corroborates to the workspace volume. Increasing L_2 has the opposite effect, although it again increases the reach of the pantograph, this time it also brings the platform closer to the rotation axis. Increasing the radius of the base, (R), moves the pantograph assembly away from the drone so it directly corroborates to highest increase in the workspace volume.

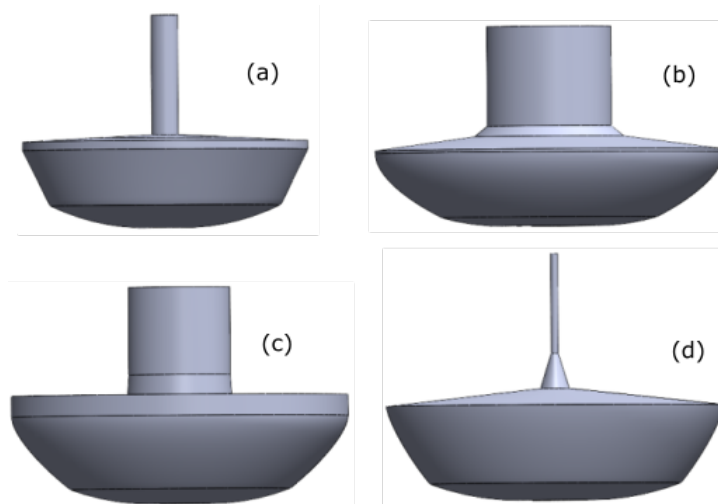


Figure C.3: Change in the workspace volume with changing parameters. (a) Increasing r , (b) Increasing R , (c) Increasing L_1 , (d) Increasing L_2

Since the mass of individual links was not considered, the links could be indefinitely increased which could, in principle, result in the largest workspace. However, the link masses have to be considered as

the upper limit on the weight of the manipulator is set 2 Kgs. Considering masses of links such that the manipulator remains balanced, is within the 2 Kg upper limit and workspace is maximum the following favorable values were found. $R = 280mm, L_1 = 170mm, L_2 = 130mm$ and $r = 180mm$. The optimized workspace is shown in fig[Figure number]

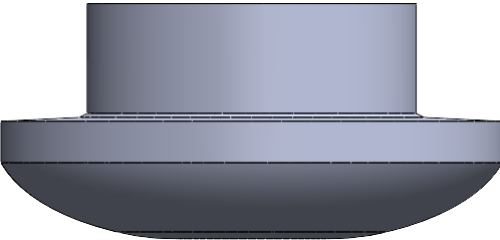
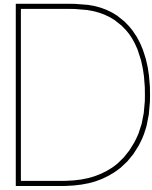


Figure C.4: Optimized workspace with favorable values



Simulations on a pantograph and further simplified model of ADAPT

D.1. Pantograph

During preliminary testing it was observed that the model did not show complete balancing but showed a deviation in the order of 10^{-5} . To interpret the result better, a simple pantograph was designed which fulfilled the force balanced conditions (Eq.3, Chapter3). The CoM of the longer links in the pantograph were artificially put outside such that the design could be less complex (Fig.D.1). The results showed

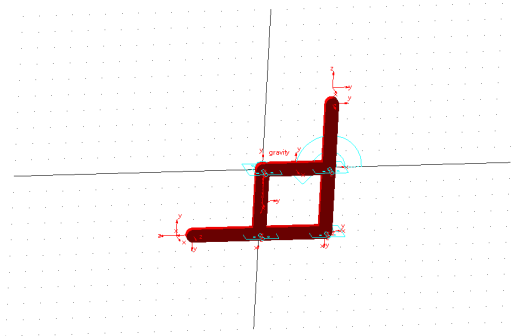


Figure D.1: MSC ADAMS model of a forced balanced pantograph. The CoMs of the longer links have been artificially put outside the links so that they fulfill the force balance conditions. The CoM is represented by the frames in MSC ADAMS

that there was error even in the simple model of a pantograph of the order of 10^{-11} (Fig. D.2). This can be explained by the quantization errors (Round off error, Discretization error, Truncation error) in numerical multi-body simulations. Although the error is quite small, a better step size can be used to reduce the total error even further.

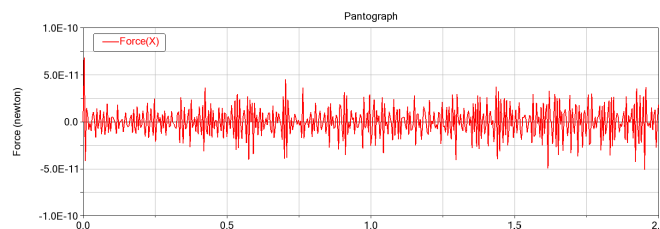


Figure D.2: Forces in the X direction for a pantograph. The shorter link is turned anti-clockwise in the simulation that extends the arms of the pantograph.

D.2. Further simplified model

In the further simplified model, the motors and counter masses were considered point masses at the same location as the CoM in the actual setup.

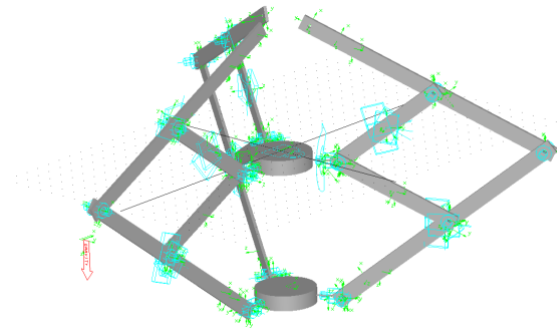
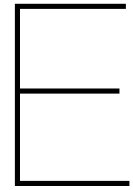


Figure D.3: The further simplified model of the manipulator with CoMs put artificially at points where they would exist if there were masses and motors like in the real system.

The numerical error in the further simplified simulation was in the same order as in the simplified model. Therefore, the simplified design was deemed sufficient for determining the reaction forces.



LabVIEW Block Diagram and User Interface

The labview data acquisition file were created taking help from Mr.Jacques Brenkman from the Meetshop, 3ME, TU Delft.

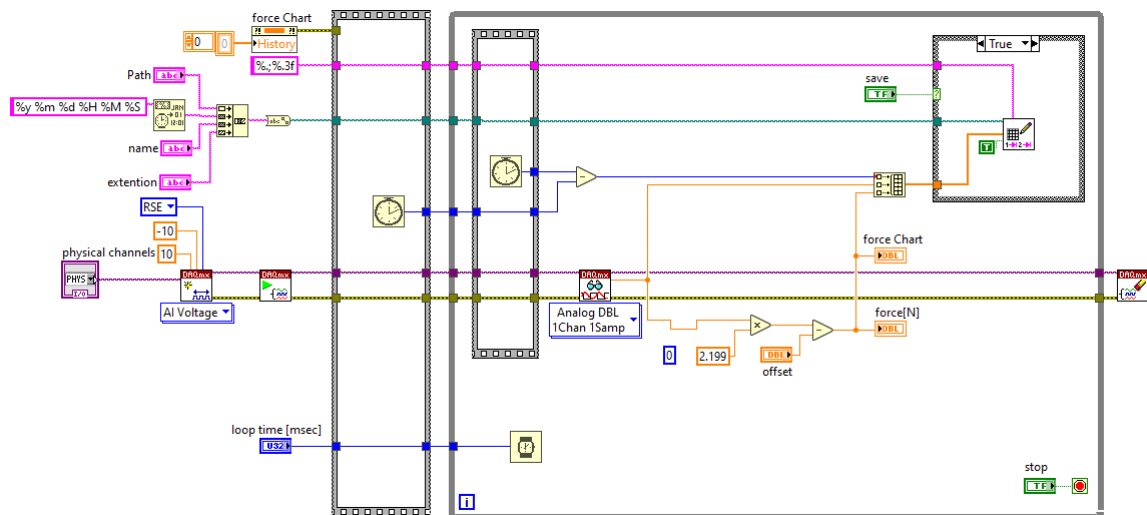


Figure E.1: The LABVIEW block diagram for single channel data acquisition

The user interface allowed to save the file to a specified directory with .csv extension that allowed easy plotting. The data was acquired every 100ms. An offset could also be set which allowed the new zero.

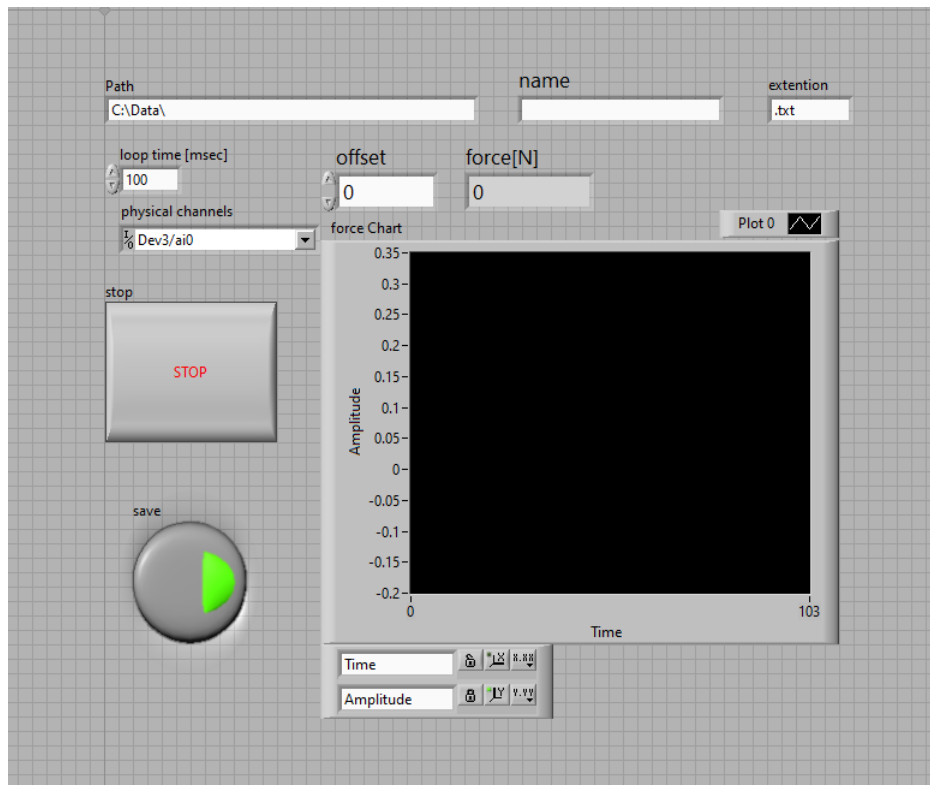


Figure E.2: The LABVIEW User Interface